

# Local and Global Analysis of Parametric Solid Sweeps

Bharat Adsul, Jinesh Machchhar, Milind Sohoni

ABSTRACT. In this work, we propose a structured computational framework for modelling the envelope of the swept volume, that is the boundary of the volume obtained by sweeping an input solid along a trajectory of rigid motions. Our framework is adapted to the well-established industry-standard brep format to enable its implementation in modern CAD systems. This is achieved via a “local analysis”, which covers parametrizations and singularities, as well as a “global theory” which tackles face-boundaries, self-intersections and trim curves. Central to the local analysis is the “funnel” which serves as a natural parameter space for the basic surfaces constituting the sweep. The trimming problem is reduced to the problem of surface-surface intersections of these basic surfaces. Based on the complexity of these intersections, we introduce a novel classification of sweeps as decomposable and non-decomposable. Further, we construct an *invariant* function  $\theta$  on the funnel which efficiently separates decomposable and non-decomposable sweeps. Through a geometric theorem we also show intimate connections between  $\theta$ , local curvatures and the inverse trajectory used in earlier works as an approach towards trimming. In contrast to the inverse trajectory approach of testing points,  $\theta$  is a computationally robust global function. It is the key to a complete structural understanding, and an efficient computation of both, the singular locus and the trim curves, which are central to a stable implementation. Several illustrative outputs of a pilot implementation are included.

*Keywords:* Solid sweep; boundary representation; parametric curves and surfaces; solid modeling

## 1. Introduction

This paper is motivated by the need for a robust implementation of solid sweeps in solid modeling kernels. The solid sweep is of course, the envelope surface of a solid which is swept in space by a family of rotations and translations. The uses of sweeps are many, e.g., in the design of scrolls [10], in CNC machining verification [14, 15], to detect collisions, and so on. Constant radius blends can be considered as the partial envelope of a sphere moving along a specified path. As with blends [6], it is expected that a deeper mathematical understanding of solid sweep will lead to its rapid deployment and use.

A robust implementation of solid sweep poses the following requirements: (i) allow for input models specified in the industry-standard brep format, (ii) output the sweep envelope in the brep format, with effective evaluators, and finally, (iii)

perform body-check, i.e., a check on the orientability, non-self-intersection, detection of singularities and so on. Thus there are some “local” parts and some “global” parts to a robust implementation of sweeps.

It is generally recognized that the harder parts of the local theory is in the smooth case, i.e., when faces of the swept solid meet each other smoothly. For in the non-smooth case, the added complexity in the local geometry of the sweep is exactly that of a curve moving in 3-space. This is of course well understood, and offered by many kernels as a basic surface type. As far as we know, the global situation in the non-smooth case, i.e., the topological structure of edges and vertices (i.e., the 1-cage) of the sweep has not been elucidated, but is also generally assumed to be simpler than the smooth case. In fact, much of existing literature has focused on a smooth single-face solid, as the key problem [1, 3, 4].

In this paper, we focus on the smooth multi-face solid. In Section 2, we start with the mathematical structure of the simple sweep (i.e., one without singularities and self-intersections). By the calculus of curves of contact, we set up a correspondence between the faces, edges and vertices of the envelope with those of the swept solid. This sets up the brep structure of the envelope. Next, we define the funnel as the parametrization space of a face of the envelope and construct a parametrization. We further elucidate the structure of the bounding edges/vertices of a face and provide several examples of simple sweeps from a pilot implementation.

In Section 3, we examine the trim structures. The funnel of Section 2 will remain the ambient parametrization of the faces. The correspondence will help us define the trim areas and trim curves which must be excised to form the correct envelope. We then define the function  $\ell$  and use it to define elementary and singular trim curves.

In Section 4, we start with the decomposable sweep, i.e., one which may be partitioned into a suitable small collection of simple sweeps. In principle, the final envelope may be obtained by stable (transversal) boolean operations on this collection. We show that the trim curves so obtained are elementary. We next define a global invariant  $\theta$  on the funnel, which is robustly and efficiently computable on the funnel and we show that  $\theta > 0$  on (all) the funnels characterizes decomposability. This is an important step in the robust implementation of sweeps.

In Section 5, we prove some of the geometric properties of  $\theta$  such as its invariance and show that it is the determinant of the transformation connecting two 2-frames on the envelope, and is thus an easily computable function on the surface. We show that the  $\theta = 0$  curve on the funnel is also the singular locus for the envelope surface. We also show the relation of  $\theta$  with the inverse trajectory [4].

In Section 6, we analyse the singular trim curve, i.e., where  $\ell$  may hit zero. We show that there is a correspondence between singular trim curves and the curves in the zero-locus of  $\theta$ . We also show that (i) singular trim curves make contact with the  $\theta = 0$  curves, and (ii) excision at the singular trim curves excises all singularities of the envelope except at these points of contact. These points themselves are easily and robustly computed.

In Section 7 we summarize what has been achieved, viz., that the decomposability and the zero-locus of  $\theta$  complement to give a complete understanding of all trim curves. We illustrate this through some examples. Finally, we outline future work.

**Previous work**

We now review existing related work. Perhaps the most elaborate proposal for the sweep surface  $\mathcal{E}$  is the sweep envelope differential equations [3] approach, where the authors (i) assume that surface  $S$  being swept is implicitly given by a function  $f$ , and (ii) derive a differential equation whose solution is the envelope. For any point  $p$  on the initial curve of contact, a Runge-Kutta marching yields a trajectory  $p(t)$  such that (i)  $p(0) = p$ , and (ii)  $p(t) \in C(t)$ , the curve of contact at time  $t$ . These trajectories presumably serve as the iso-parametric lines  $p(t) = \mathcal{E}(t, u(p))$ . Determining whether  $p(t)$  is in the trimming set  $T$  is solved by using the inverse trajectory condition. This is implemented by using the second derivative of the function  $\phi(x, t) = f(\eta(x, t))$ , where  $\eta$  is the inverse trajectory of point  $x$ .

On the global front, the building of the envelope  $\mathcal{E}$  is done by selecting a collection of points on the initial curve of contact, developing trajectories, testing for membership in  $T$  and then using the points which pass to construct an approximation to the envelope. The drawbacks are clear. Typically, when  $S$  is presented as a brep, constructing an  $f$  which defines  $S$  is difficult. Furthermore, the choice of  $f$  seems to determine many computational and parametric issues, which is undesirable. The inverse-trajectory check remains poorly conditioned, especially when the second derivative of the function  $\phi(x, t)$  w.r.t.  $t$  is zero, a situation which arises repeatedly. The structure of the envelope is unknown at a point where this derivative is zero. A global understanding of  $T$  and the nature of the trim curves is missing. A surface is fit through the points which pass the inverse trajectory test. Hence, an important feature, namely,  $G1$ -discontinuity along the trim curve on the envelope is missed out by this method. Further, since only sampled points are subjected to inverse trajectory test, some portion of the trimming set  $T$  may be left undetected.

In [7], the authors give a membership test for a point in the object space to belong inside, outside or on the boundary of the swept volume. This is done by studying the interaction of inverse trajectory of the point in question with the solid at initial position. A curve-solid intersection is required to be computed for each point membership query which is computationally expensive, especially when the intersection is non-transversal, as noted by the authors. Further, this approach yields a procedural implicit representation of the envelope. In practice, a parametric representation is often desirable so that it is efficient to produce points on the envelope.

In [8] the authors work with 2D shapes and 2D motions and quantify singularities using inverse trajectories. This work is based on the computational framework described in [7] and involves computing intersections between 2D curves and 2D shapes. The authors remark that this work can be extended to the 3-dimensional case involving intersections between 3D curves and 3D solids. This approach has the same drawback as [7], namely a high computational cost and the obvious limitation of dimensionality.

In trimming self-intersections in swept volumes [17], the authors detect self-intersections by computing approximate curves of contact at a few discrete time instances which are then checked for intersections. Approximations are introduced at multiple levels, hence such an approach is not likely to meet the accuracy standards of most CAD kernels.

In [9], the authors approximate the given trajectory by a continuous, piecewise screw motion and generate candidate faces of the swept surface. In order to performing trimming, inverse trajectory is used. Limitation of this method is clear, namely, restricted class of motions along which the sweep occurs.

In [16], the authors present an error-bounded approximation of the envelope of the volume swept by a polyhedron along a parametric trajectory. Authors use volumetric approach using adaptive grid to provide guarantee about the correctness of the topology of the swept volume. This approach, however, cannot be readily extended to sweep smooth solids.

## 2. Mathematical structure of sweeps

In this section we formulate the boundary of the volume obtained by sweeping a solid  $M$  along a given trajectory  $h$ .

**2.1. Correspondence and brep structure of envelope.** We will use the boundary representation, also known as brep, which is a popular standard for representing a compact and oriented solid  $M$  by its boundary  $\partial M$ . The boundary  $\partial M$  separates the interior of  $M$  from the exterior of  $M$  and is represented using a set of *faces*, *edges* and *vertices*. See Figure 1 for the brep of a solid where different faces are colored differently. Faces meet in edges and edges meet in vertices. The brep consists of two interconnected pieces of information, viz., the geometric and the topological. The geometric information consists of the parametric description of the faces and edges while the topological information consists of orientation of the geometric entities and adjacency relations between them.

In this paper we consider solids whose boundary is formed by faces meeting smoothly. In the case when the faces do not meet smoothly, the added complexity in the local geometry of the sweep is exactly that of a curve moving in 3-space. This is of course well understood, and offered by many kernels as a basic surface type. The global geometry and topology for this case will be described in a later paper.

DEFINITION 1. A **trajectory** in  $\mathbb{R}^3$  is specified by a map

$$h : I \rightarrow (SO(3), \mathbb{R}^3), h(t) = (A(t), b(t))$$

where  $I$  is a closed interval of  $\mathbb{R}$ ,  $A(t) \in SO(3)$ <sup>1</sup>,  $b(t) \in \mathbb{R}^3$ . The parameter  $t$  represents time.

We assume that  $h$  is of class  $C^k$  for some  $k \geq 2$ , i.e., partial derivatives of order up to  $k$  exist and are continuous.

We make the following key assumption about  $(M, h)$ .

ASSUMPTION 2. *The tuple  $(M, h)$  is in a general position.*

DEFINITION 3. The **action** of  $h$  (at time  $t$  in  $I$ ) on  $M$  is given by  $M(t) = \{A(t) \cdot x + b(t) | x \in M\}$ . The **swept volume**  $\mathcal{V}$  is the union  $\bigcup_{t \in I} M(t)$  and the

**envelope**  $\mathcal{E}$  is defined as the boundary of the swept volume  $\mathcal{V}$ .

Clearly, for each point  $y$  of  $\mathcal{E}$  there must be an  $x \in M$  and a  $t \in I$  such that  $y = A(t) \cdot x + b(t)$ . This sets up the following correspondence relation.

---

<sup>1</sup> $SO(3) = \{X \text{ is a } 3 \times 3 \text{ real matrix} | X^t \cdot X = I, \det(X) = 1\}$  is the special orthogonal group, i.e. the group of rotational transforms.

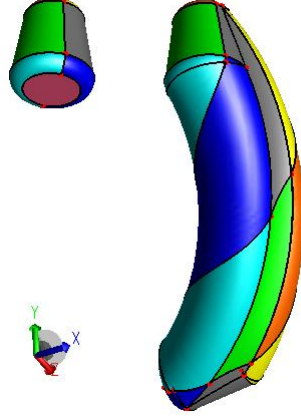


FIGURE 1. The envelope of a cone with blended edges being swept along a helical trajectory with compounded rotation.

DEFINITION 4. The **correspondence**  $R$  is the set of tuples

$$R = \{(y, x, t) \in \mathcal{E} \times M \times I \mid y = A(t) \cdot x + b(t)\}$$

For  $t_0 \in I$ , we set  $R_{t_0} := \{(y, x, t) \in R \mid t = t_0\}$ . Similarly, for  $y_0 \in \mathcal{E}$ , we define  ${}_{y_0}R := \{(y, x, t) \in R \mid y = y_0\}$ .

We will denote the interior of a set  $W$  by  $W^\circ$ . It is clear that  $\mathcal{V}^\circ = \cup_{t \in I} M(t)^\circ$ . Therefore, we have

LEMMA 5. *If  $x \in M^\circ$ , then for all  $t \in I$ ,  $A(t) \cdot x + b(t) \notin \mathcal{E}$ .*

Thus, the points in the interior of  $M$  do not contribute to  $\mathcal{E}$  at all and  $R \subset \mathcal{E} \times \partial M \times I$ .

LEMMA 6. *Assuming general position of  $(M, h)$ , for any  $y \in \mathcal{E}$ , there are at most three distinct tuples  $(y, x_i, t_i)$  for  $i = 1, 2, 3$  which belong to  ${}_yR$ .*

*Proof.* For distinct tuples  $(y, x_1, t_1), (y, x_2, t_2) \in {}_yR$ , it is clear that  $t_1 \neq t_2$ , for otherwise  $x_1 = x_2$ . Therefore  $\partial M(t_1)$  and  $\partial M(t_2)$  intersect at point  $y$ . By Assumption 2 this intersection is transversal. Further, by the same assumption, at most 3 surfaces may intersect in a point.  $\square$

It will be shown in the coming sections that for almost all points  $y \in \mathcal{E}$  there is exactly one tuple  $(y, x, t)$  in  ${}_yR$ . This sets up the brep structure for  $\mathcal{E}$ . In the sweep example shown in Figure 1, the correspondence  $R$  is illustrated via color coding, i.e., for  $(y, x, t) \in R$ , the points  $y$  and  $x$  are shown in the same color. The general position assumption on  $(M, h)$  can be formulated as the condition that the induced brep topology of  $\mathcal{E}$  remains invariant under a small perturbation of  $(M, h)$ .

DEFINITION 7. For a point  $x \in M$ , define the **trajectory of  $x$**  as the map  $\gamma_x : I \rightarrow \mathbb{R}^3$  given by  $\gamma_x(t) = A(t) \cdot x + b(t)$  and the velocity  $v_x(t)$  as  $v_x(t) = \gamma'_x(t) = A'(t) \cdot x + b'(t)$ .

For a point  $x \in \partial M$ , let  $N(x)$  be the unit outward normal to  $M$  at  $x$ . Define the function  $g : \partial M \times I \rightarrow \mathbb{R}$  as

$$(1) \quad g(x, t) = \langle A(t) \cdot N(x), v_x(t) \rangle$$

Thus,  $g(x, t)$  is the dot product of the velocity vector with the unit normal at the point  $\gamma_x(t) \in \partial M(t)$ .

Proposition 8 gives a necessary condition for a point  $x \in \partial M$  to contribute a point on  $\mathcal{E}$  at time  $t$ , namely,  $\gamma_x(t)$ , and is a rewording in our notation of the statement in [3] that *the candidate set is the union of the ingress, the egress and the grazing set of points*.

PROPOSITION 8. *For  $(y, x, t) \in R$  and  $I = [t_0, t_1]$ , either (i)  $g(x, t) = 0$  or (ii)  $t = t_0$  and  $g(x, t) \leq 0$ , or (iii)  $t = t_1$  and  $g(x, t) \geq 0$ .*

For the proof, refer Appendix A.

DEFINITION 9. For a fixed time instant  $t_0 \in I$ , the set  $\{\gamma_x(t_0) | x \in \partial M, g(x, t_0) = 0\}$  is referred to as the **curve of contact** at  $t_0$  and denoted by  $C_I(t_0)$ . Observe that  $C_I(t_0) \subset \partial M(t_0)$ . The union of the curves of contact is referred to as the **contact set** and denoted by  $C_I$ , i.e.,  $C_I = \bigcup_{t \in I} C_I(t)$ .

In the sweep example in Figure 4, the curve of contact at  $t = 0$  is shown imprinted on the solid in red. The curves of contact are referred to as the *characteristic curves* in [13].

DEFINITION 10. Define projections  $\tau : R \rightarrow I$  and  $Y : R \rightarrow \mathcal{E}$  as:  $\tau(y, x, t) = t$  and  $Y(y, x, t) = y$ .

DEFINITION 11. A sweep  $(M, h, I)$  is said to be **simple** if for all  $t \in I^\circ$ ,  $C_I(t) = Y(R_t)$ .

Note that, by Proposition 8, for any sweep, we have  $Y(R_t) \subseteq C_I(t)$  for all  $t \in I^\circ$ . In a simple sweep, we require that  $C_I(t) = Y(R_t)$ . In other words, every point on the contact-set appears on the envelope, and thus, no *trimming* of the contact-set is needed in order to obtain the envelope.

LEMMA 12. *For a simple sweep, for all  $y \in \mathcal{E}$ ,  ${}_yR$  is a singleton set.*

*Proof.* We first show that for a simple sweep, for  $t \neq t'$ ,  $C_I(t) \cap C_I(t') = \emptyset$ . Suppose that  $y \in C_I(t) \cap C_I(t')$ . Clearly,  $C_I(t) \subset \partial M(t)$  and  $C_I(t') \subset \partial M(t')$ . Hence  $y \in \partial M(t) \cap \partial M(t')$ . By Assumption 2 about the general position of  $(M, h)$ ,  $\partial M(t)$  and  $\partial M(t')$  intersect transversally. Hence  $C_I(t) \cap M^\circ(t') \neq \emptyset$  and  $C_I(t') \cap M^\circ(t) \neq \emptyset$ . It follows by Lemma 5 that  $C_I(t) \not\subset Y(R_t)$  and  $C_I(t') \not\subset Y(R_{t'})$  which contradicts the fact that  $(M, h, I)$  is simple.

Now suppose that there are 2 tuples  $(y, x_i, t_i) \in {}_yR$  for  $i = 1, 2$ . Since  $\partial M$  is free from self-intersections it follows that  $t_1 \neq t_2$  and  $y \in C_I(t_1) \cap C_I(t_2)$  which is a contradiction to the fact that  $(M, h, I)$  is simple.  $\square$

**2.2. Parametrizations.** Now we describe parametrizations of the various entities of the induced brep structure of  $\mathcal{E}$ . Here we restrict to the case of the simple sweep. The more general case is derived from this.

2.2.1. *Geometry of faces of  $\mathcal{E}$ .* Let  $F$  be a face of  $\partial M$ . In general,  $F$  gives rise to a set of faces of  $\mathcal{E}$ . Below we describe a natural parametrization of these faces using the parametrization of the surface underlying the face  $F$ .

DEFINITION 13. A **smooth/regular parametric surface** in  $\mathbb{R}^3$  is a smooth map  $S : \mathbb{R}^2 \rightarrow \mathbb{R}^3$  such that at all  $(u_0, v_0) \in \mathbb{R}^2$   $\frac{\partial S}{\partial u}|_{(u_0, v_0)} \in \mathbb{R}^3$  and  $\frac{\partial S}{\partial v}|_{(u_0, v_0)} \in \mathbb{R}^3$  are linearly independent. Here  $u$  and  $v$  are called the parameters of the surface.

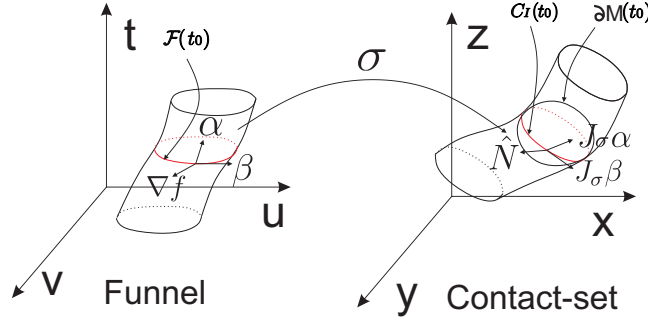


FIGURE 2. The funnel and the contact-set.

Let  $S$  be the regular surface underlying the face  $F$  of  $\partial M$ .

DEFINITION 14. Define the function  $f : \mathbb{R}^2 \times I \rightarrow \mathbb{R}$  as  $f(u, v, t) = g(S(u, v), t)$ .

The domain of function  $f$  will be referred to as the parameter space. Note that  $f$  is easily and robustly computed.

DEFINITION 15. For an interval  $I = [t_0, t_1]$ , we define the following subsets of the parameter space

$$\begin{aligned} \mathcal{L} &= \{(u, v, t) \in \mathbb{R}^2 \times \{t_0\} \text{ such that } f(u, v, t) \leq 0\} \\ \mathcal{F} &= \{(u, v, t) \in \mathbb{R}^2 \times I \text{ such that } f(u, v, t) = 0\} \\ \mathcal{R} &= \{(u, v, t) \in \mathbb{R}^2 \times \{t_1\} \text{ such that } f(u, v, t) \geq 0\} \end{aligned}$$

The set  $\mathcal{F}$  will be referred to as the **funnel**.

By Assumption 2 about the general position of  $(M, h)$  it follows that for all  $p \in \mathcal{F}$ , the gradient  $\nabla f(p) = [f_u(p), f_v(p), f_t(p)]^T \neq \bar{0}$ . As a consequence,  $\mathcal{F}$  is a smooth, orientable surface in the parameter space.

DEFINITION 16. The set  $\{(u, v, t) \in \mathcal{F} | t = t_0\}$  will be referred to as the **p-curve of contact** at  $t_0$  and denoted by  $\mathcal{F}(t_0)$ .

We now define the sweep map from the parameter space to the object space.

DEFINITION 17. The **sweep map** is defined as follows.

$$\sigma : \mathbb{R}^2 \times I \rightarrow \mathbb{R}^3, \sigma(u, v, t) = A(t) \cdot S(u, v) + b(t)$$

Note that,  $\sigma$  is a smooth map,  $C_I = \sigma(\mathcal{F})$  and  $C_I(t) = \sigma(\mathcal{F}(t))$ . Here and later, by a slight abuse of notation,  $\mathcal{E}$ ,  $C_I$  and  $C_I(t)$  denote the appropriate parts of complete  $\mathcal{E}$ ,  $C_I$  and  $C_I(t)$  respectively resulting from the face  $F \subset \partial M$  whose underlying surface is  $S$ . The surface patches  $\sigma(\mathcal{L})$  and  $\sigma(\mathcal{R})$  will be referred to as the left and right end-caps respectively.

The funnel, the contact-set,  $\mathcal{F}(t_0)$  and  $C_I(t_0)$  are shown schematically in Figure 2.

The condition  $f = 0$  can also be looked upon as the rank deficiency condition [1] of the Jacobian  $J_\sigma$  of the sweep map  $\sigma$ . To make this precise, let

$$(2) \quad J_\sigma = [\sigma_u \quad \sigma_v \quad \sigma_t]_{3 \times 3}$$

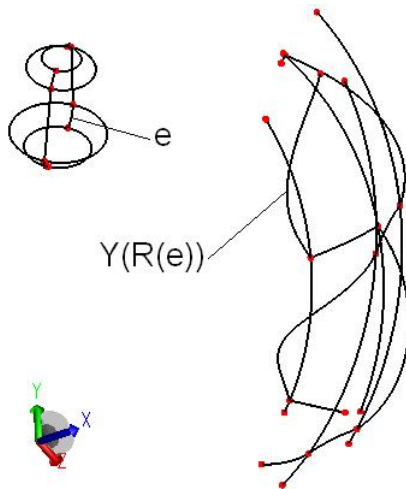


FIGURE 3. The edges of envelope for the sweep example shown in Figure 1.

where  $\sigma_u = A(t) \cdot \frac{\partial S}{\partial u}(u, v)$ ,  $\sigma_v = A(t) \cdot \frac{\partial S}{\partial v}(u, v)$  and  $\sigma_t = A'(t) \cdot S(u, v) + b'(t)$ . Note that if  $S(u, v) = x$  then  $\sigma_t = \gamma'_x(t)$  is the velocity, also denoted by  $V(u, v, t)$ . Observe that regularity of  $S$  ensures that  $J_\sigma$  has rank at least 2. Further, it is easy to show that  $f(u, v, t)$  is a non-zero scalar multiple of the determinant of  $J_\sigma$ . Therefore, the condition  $f = 0$  is precisely the rank deficiency condition of  $J_\sigma$ .

For a simple sweep, by Proposition 8, Definition 11 and Definition 15 it follows that  $\mathcal{E} = \sigma(\mathcal{L} \cup \mathcal{F} \cup \mathcal{R})$ . The surface patches  $\sigma(\mathcal{L})$  and  $\sigma(\mathcal{R})$  can be obtained from  $\partial M$  using Proposition 8 and Definition 15. The *trim curve* in parameter space for  $\sigma(\mathcal{L})$  is given by  $f(u, v, t_0) = 0$  and that for  $\sigma(\mathcal{R})$  is given by  $f(u, v, t_1) = 0$ .

We now come to the parametrization of  $\sigma(\mathcal{F}) = C_I$ . The non-singularity of  $f$  makes  $\mathcal{F}$  an effective parametrization space for  $C_I$ . Since time  $t$  is a central parameter of the sweep problem and is important in numerous applications, it is useful to have  $t$  as one of the parameters of  $C_I$ . Since in a simple sweep,  $\sigma|_{\mathcal{F}} : \mathcal{F} \rightarrow C_I$  is a diffeomorphism onto its image, we may address the problem of parameterizing  $C_I$  by parameterizing the funnel  $\mathcal{F}$ . For most non-trivial sweeps there is no closed form solution for the parametrization of the envelope and we address this problem using the procedural paradigm which is now standard in many kernels and is described in Appendix C. In this approach, a set of evaluators are constructed for the curve/surface via numerical procedures which converge to the solution up to the required tolerance. This has the advantage of being computationally efficient as well as accurate.

We now look at the bounding edges of the faces resulting from the face  $F$  of  $\partial M$ , which are generated by the bounding edges of  $F$ .

2.2.2. *Geometry of edges of  $\mathcal{E}$ .* We now briefly describe the computation of edges of  $\mathcal{E}$  via the correspondence  $R$ . If  $\partial M$  is composed of faces meeting smoothly, an edge  $e$  of  $\partial M$  will, in general, give rise to a set of edges in  $\mathcal{E}$ . We define the restriction of  $R$  to the edge  $e$  as follows.

DEFINITION 18. For an edge  $e \in \partial M$ , define  $R(e) = \{(y, x, t) \in R | x \in e\}$ .

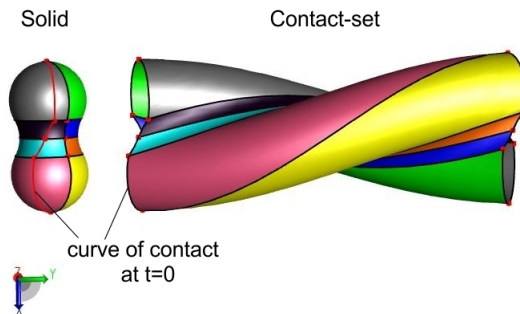


FIGURE 4. The envelope(without end-caps) of a dumbbell undergoing translation along  $y$ -axis and undergoing rotation about  $y$ -axis.

Let  $e$  be the intersection of faces  $F_1$  and  $F_2$  in  $\partial M$  and let  $s$  denote the parameter of  $e$ . Since  $F_1$  and  $F_2$  meet smoothly at  $e$ , at every point  $e(s)$  of  $e$  there is a well-defined normal. Hence we may define the following function on the parameter space  $\mathbb{R} \times I$ .

DEFINITION 19. Define the function  $f^e : \mathbb{R} \times I \rightarrow \mathbb{R}$  as  $f^e(s, t) = g(e(s), t)$ .

Note that the function  $f^e$  is the restriction of the function  $f$  defined in Definition 14 to the parameter space curve  $(u(s), v(s))$  corresponding to the edge  $e$  so that  $e(s) = S(u(s), v(s))$  where  $S$  is the surface underlying face  $F_1$ . The following Lemma gives a necessary condition for a point  $e(s)$  to be on  $\mathcal{E}$  at time  $t$ .

LEMMA 20. For  $(y, e(s), t) \in R(e)$  and  $I = [t_0, t_1]$ , either (i)  $t = t_0$  and  $f^e(s, t) \leq 0$ , or (ii)  $t = t_1$  and  $f^e(s, t) \geq 0$  or (iii)  $f^e(s, t) = 0$ .

*Proof.* This follows from Prop. 8 and Definition 19.  $\square$

Figure 3 shows the edges of the envelope for the sweep example shown in Figure 1. The correspondence for one of the edges of the envelope is also marked.

Let  $\mathcal{F}_1$  denote the funnel corresponding to the contact set generated by face  $F_1$ . The edge in parameter space which bounds  $\mathcal{F}_1$  is given by  $\{(u(s), v(s), t) \in \mathbb{R}^2 \times I | f^e(s, t) = 0\}$  which we will denote by  $\mathcal{F}^e$ . Note that  $\mathcal{F}^e$  is smooth if  $(f_s^e, f_t^e) = (f_u \cdot u_s + f_v \cdot v_s, f_t) \neq (0, 0)$  at all points in  $\mathcal{F}^e$ .

2.2.3. *Geometry of vertices of  $\mathcal{E}$ .* A vertex  $z$  on  $\partial M$  will, in general, give rise to a set of vertices on  $\mathcal{E}$ . We further restrict the correspondence  $R$  to  $z$  as  $R(z) = \{(y, x, t) \in R | x = z\}$ . As  $\partial M$  is smooth, there is a well-defined normal at  $z$ . Hence we may define the function  $f^z : I \rightarrow \mathbb{R}$  as  $f^z(t) = g(z, t)$ . If  $z$  is on the boundary of a face  $F_1$ ,  $z$  will have a set of coordinates in the parameter space of the surface  $S$  underlying the face  $F_1$ , say  $(u_0, v_0)$ , so that  $z = S(u_0, v_0)$ . It is easy to see that if  $(y, z, t) \in R(z)$  and  $I = [t_0, t_1]$  then either (i)  $t = t_0$  and  $f^z(t) \leq 0$ , or (ii)  $t = t_1$  and  $f^z(t) \geq 0$  or (iii)  $f^z(t) = 0$ .

**2.3. Examples of simple sweeps.** Three examples of simple sweeps are shown in Figures 4, 5 and 6 which were generated using a pilot implementation of our algorithm in the ACIS 3D Modeler [2]. A curve of contact at the initial time is shown imprinted on the solid in Figure 4.

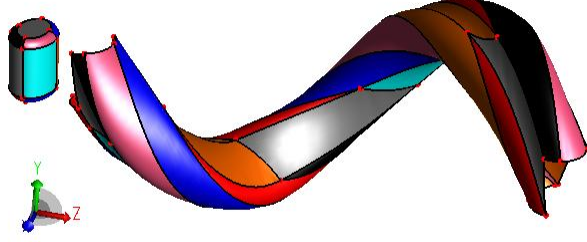


FIGURE 5. The envelope(without end-caps) of an elliptical cylinder undergoing a screw motion while rotating about its own axis.

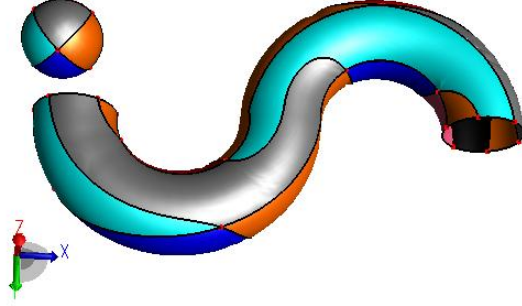


FIGURE 6. The envelope(without end-caps) of a sphere sweeping along an 'S' shaped trajectory while rotating about  $y$ -axis

### 3. The trim structures

Unlike in a simple sweep, all points of  $C_I$  may not belong to the envelope. Figure 7 shows an example of such a sweep. In Figure 7(b) the contact set restricted to the later half of the sweep interval is shown after removing the set of points which does not belong to the envelope. We now define the subset of  $C_I$  which needs to be excised in order to obtain  $\mathcal{E}$ .

DEFINITION 21. The **trim set** is defined as

$$T_I := \{x \in C_I \mid \exists t \in I, x \in M^o(t)\}$$

By Lemma 5 it is clear that  $T_I \cap \mathcal{E} = \emptyset$ . The correspondence in Definition 4 does not capture the points of  $C_I$  which do not belong to the envelope. In order to identify such points, we extend the correspondence of Definition 4 to  $C_I \times M \times I$  as below.

DEFINITION 22. Let  $\tilde{R} := \{(y, x, t) \in C_I \times M \times I \mid y = A(t) \cdot x + b(t)\}$ . As expected, we define  $\tau : \tilde{R} \rightarrow I$  and  $Y : \tilde{R} \rightarrow C_I$  as:  $\tau(y, x, t) = t$  and  $Y(y, x, t) = y$ . Further, as before,  $\tilde{R}_{t_0} := \{(y, x, t) \in \tilde{R} \mid t = t_0\}$ ,  ${}_{y_0}\tilde{R} := \{(y, x, t) \in \tilde{R} \mid y = y_0\}$ .

A crucial observation is that, unlike the earlier correspondence,  $\tilde{R} \not\subset C_I \times \partial M \times I$  simply because  $\tilde{R}$  may contain a tuple  $(y, x, t)$  where  $x \in M^o$ . In other words, for

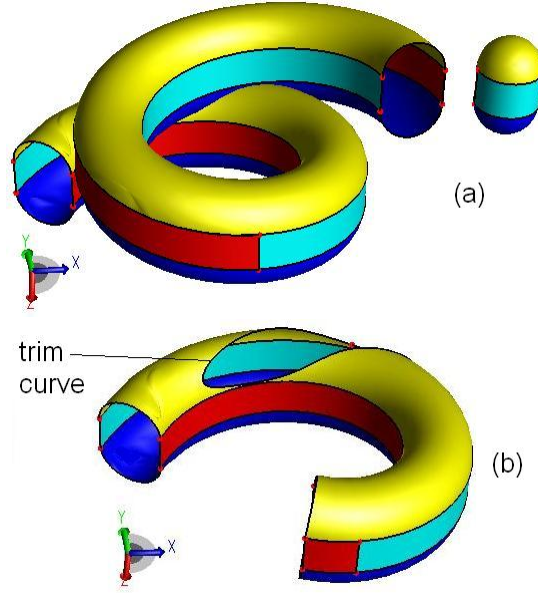


FIGURE 7. (a) The contact set of a capsule moving along a helix while rotating about  $y$ -axis.(b) The contact set restricted to interval  $[0.5, 1.0]$  with the trim set excised.

$x' \in \partial M$  and  $y = \gamma_{x'}(t') \in C_I$ , it may happen that  $\gamma_{x'}(t') = \gamma_x(t)$  for some  $t \neq t'$  and some  $x \in M^\circ$ . In this case,  ${}_y\tilde{\mathcal{R}}$  will not be a singleton set.

LEMMA 23. *The set  $T_I$  is open in  $C_I$ .*

*Proof.* Consider a point  $y_0 \in T_I$ . Then  $y_0 \in M^\circ(t_0)$  for some  $t_0 \in I$ . Hence, there exists an open ball of non-zero radius  $r$  centered at  $y_0$ , denote it by  $B(y_0, r)$ , which is itself contained in  $M^\circ(t_0)$ . Let  $\mathcal{N}_0 := B(y_0, r) \cap C_I$ . Then,  $\mathcal{N}_0 \subset T_I$  and  $\mathcal{N}_0$  is open in  $T_I$ . Hence  $T_I$  is open in  $C_I$ .  $\square$

In general, the trim set will span several parts of  $C_I$  corresponding to different faces of  $\partial M$ . For the ease of notation and presentation, in the rest of this paper, we will analyse the corresponding trim structures on the *funnel* of a fixed face  $F$  of  $\partial M$ . Thanks to the natural parametrizations (cf. subsection 2.2), the migration of these trim structures across different funnels is an easy implementation detail. In view of this, we carry forward the notation developed in subsection 2.2.1 through the rest of this paper.

DEFINITION 24. The pre-image of  $T_I$  on the funnel under the map  $\sigma$  will be referred to as the **p-trim set**, denoted by  $pT_I$ , i.e.,  $pT_I = \sigma^{-1}(T_I) \cap \mathcal{F}$ .

An immediate corollary of Lemma 23 is:  $pT_I$  is open in  $\mathcal{F}$ .

One can also define similar parametric trim areas on the left and right caps (cf.  $\mathcal{L}$  and  $\mathcal{R}$  from Definition 15) and their counterparts in the object space. However, in this paper, we assume here that these trim structures are empty. Our analysis can be extended to also cover the non-empty case.

DEFINITION 25. The boundary of  $\overline{T_I}$  will be referred to as the **trim curves** and denoted by  $\partial T_I$ . Here  $\overline{T_I}$  denotes the closure of  $T_I$  in  $C_I$ . Similarly, the boundary

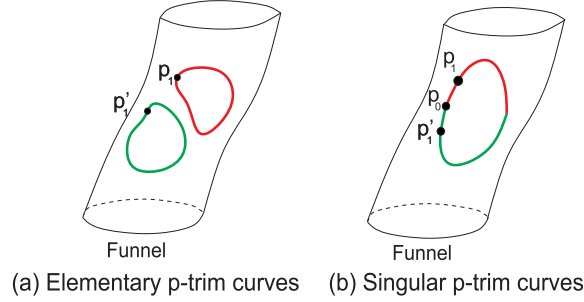


FIGURE 8. Elementary and singular p-trim curves.

of the closure  $\overline{pT_I}$  of  $pT_I$  in  $\mathcal{F}$  will be referred to as the **p-trim curves** and denoted by  $\partial pT_I$ .

Note that  $\mathcal{E} \cap T_I = \emptyset$ ,  $\mathcal{E} \cap \overline{T_I} = \partial T_I$  and  $\sigma(\mathcal{F} \setminus pT_I) = \mathcal{E}$ . Since  $\partial T_I$  forms the boundary of the trim set, the problem of excising the trim set is reduced to the problem of computing the trim curves. Further, this computation is eventually reduced to *guided* parametric surface-surface intersections via the parametrization of  $\sigma(\mathcal{F})$  described in Section 2.2. In order to characterize the points of  $\partial pT_I$  we define the following function.

**DEFINITION 26.** For  $p = (u, v, t) \in \mathcal{F}$ , let  $\sigma(p) = y$ . Define  $L : \mathcal{F} \rightarrow 2^{\mathbb{R}}$  as  $L(p) := \tau(y\tilde{R})$ , where  $2^{\mathbb{R}}$  denotes the set of all subsets of  $\mathbb{R}$ . In other words,  $L(p)$  is the set of all time instances  $t'$  (except  $t$ ) such that some point of  $M(t')$  coincides with  $\sigma(p)$ .

**LEMMA 27.** Let  $p_0 \in \overline{pT_I}$ . Then  $p_0 \in pT_I$  iff  $L(p_0)$  contains an interval, and  $p_0 \in \partial pT_I$  iff  $L(p_0)$  is a discrete set of cardinality either two or three.

*Proof.* Suppose first that  $p_0 \in pT_I$ . Let  $y_0 := \sigma(p_0)$ . Then  $y_0 \in T_I$  and  $y_0 \in M^o(t_0)$  for some  $t_0 \in I$ . Let  $B(y_0, r)$  be an open ball of radius  $r > 0$  centered at  $y_0$  contained in  $M^o(t_0)$ . Assume without loss of generality that  $A(t_0) = I$  and  $b(t_0) = 0$ . By continuity of the trajectory  $h$  it follows that given  $r > 0$  there exists  $\delta t > 0$  such that for all  $t \in [t_0, t_0 + \delta t]$ ,  $\|y_0 - A(t) \cdot y_0 - b(t)\| < r$ . Thus for each  $t \in [t_0, t_0 + \delta t]$ , there exists a point  $x = A^{-1}(t) \cdot (y_0 - b(t)) \in B(y_0, r)$  satisfying  $y_0 = A(t) \cdot x + b(t)$ , i.e.,  $y_0 \in M^o(t)$ . In other words,  $[t_0, t_0 + \delta t] \in L(p_0)$ .

Conversely, suppose that  $L(p_0)$  contains an interval  $[t_1, t_2]$ , i.e.,  $y_0 \in M(t)$  for all  $t \in [t_1, t_2]$ . By Assumption 2 about the general position of  $(M, h)$  it follows that  $y_0 \in M^o(t)$  for some  $t \in [t_1, t_2]$ , i.e.,  $y_0 \in T_I$  and  $p_0 \in pT_I$ . We have shown that for  $p_0 \in \overline{pT_I}$ ,  $p_0 \in pT_I$  iff  $L(p_0)$  contains an interval. Hence,  $L(p_0)$  is discrete iff  $p_0 \in \partial pT_I$ .

As  $\partial T_I \subset \mathcal{E}$ , by Lemma 6, it follows that at all but finitely many points  $p \in \partial pT_I$ ,  $L(p)$  is of cardinality 2 and at remaining points it is of cardinality 3.  $\square$

From Lemma 27 it follows that for almost all points  $y \in \partial T_I$  there are two points  $p_1, p'_1 \in \partial pT_I$  such that  $\sigma(p_1) = \sigma(p'_1) = y$ . Figure 8 schematically illustrates p-trim curves on  $\mathcal{F}$ . For every point  $p_1$  in the red portion of  $\partial pT_I$ , there is a point  $p'_1$  in the green portion of  $\partial pT_I$  such that  $\sigma(p_1) = \sigma(p'_1)$ .

DEFINITION 28. Define the function  $\ell : \mathcal{F} \rightarrow \mathbb{R} \cup \infty$  as follows. For  $p = (u, v, t) \in \mathcal{F}$ ,

$$\begin{aligned} \ell(p) &= \inf_{t' \in L(p), t' \neq t} \|t - t'\| && \text{if } L(p) \text{ is not a singleton set,} \\ &= \infty && \text{if } L(p) \text{ is a singleton set (i.e., } L(p) = \{t\}). \end{aligned}$$

Further, we define  $\mathbf{t}\text{-sep} = \inf_{p \in \mathcal{F}} \ell(p)$ .

For  $p \in \mathcal{F}$ , the function  $\ell$  gives the ‘smallest’ time  $\delta t$  such that some point of  $M(t \pm \delta t)$  coincides with  $\sigma(p)$ .

We classify trim curves as follows.

DEFINITION 29. A curve  $C$  of  $\partial pT_I$  is said to be **elementary** if there exists  $\delta > 0$  such that for all  $p \in C$ ,  $\ell(p) > \delta$ . It is said to be **singular** if  $\inf_{p \in C} \ell(p) = 0$ .

Figures 8(a) and 8(b) schematically illustrate elementary and singular p-trim curves on  $\mathcal{F}$  respectively. Further observe that,  $\mathbf{t}\text{-sep} > 0$  in case (a) and 0 in case (b). The trim curve in the example shown in Figure 7 is elementary. The trim curves in examples shown in Figures 12, 13, 14 and 15 are singular.

Before proceeding further, we introduce the following notation: for  $J \subset I$ ,  $\mathcal{F}(J) = \{(u, v, t) \in \mathcal{F} \mid t \in J\}$ .

LEMMA 30. *All but finitely many points of elementary trim curves lie on the transversal intersections of two surface patches  $\sigma(\mathcal{F}(I_i))$  and the remaining points lie on the transversal intersection of three surface patches  $\sigma(\mathcal{F}(I_i))$  where, for  $i = 1, 2, 3$ ,  $I_i \subset I$  are subintervals.*

*Proof.* Without loss of generality, assume that all curves of  $\partial pT_I$  are elementary, i.e.,  $\exists \delta > 0$  such that for all  $p \in \partial pT_I$ ,  $\ell(p) > \delta$ . By Lemma 27, all but finitely many points  $y \in \partial T_I$  have two points  $p_1 = (u_1, v_1, t_1)$  and  $p_2 = (u_2, v_2, t_2)$  in  $\partial pT_I$  such that  $\sigma(p_1) = \sigma(p_2) = y$ . Let  $\mathcal{F}_1 := \mathcal{F}([t_1 - \delta, t_1 + \delta])$  and  $\mathcal{F}_2 := \mathcal{F}([t_2 - \delta, t_2 + \delta])$ . Then  $y \in \sigma(\mathcal{F}_1) \cap \sigma(\mathcal{F}_2)$ . It will be shown later (cf. Section 5.2) that  $\partial M(t_1)$  and  $\partial M(t_2)$  are tangential to  $\sigma(\mathcal{F}_1)$  and  $\sigma(\mathcal{F}_2)$  respectively at  $y$ . By Assumption 2 about general position of  $(M, h)$ ,  $\partial M(t_1)$  and  $\partial M(t_2)$  intersect transversally at  $y$ . Hence,  $\sigma(\mathcal{F}_1)$  and  $\sigma(\mathcal{F}_2)$  intersect transversally at  $y$ .

At most finitely many points  $y \in \partial T_I$  have three points  $p_1, p_2$  and  $p_3$  in  $\partial pT_I$  such that  $\sigma(p_i) = y$ . By an argument similar to above, it can be shown that  $y$  lies on the transversal intersection of three surface patches  $\sigma(\mathcal{F}_i)$  for  $\mathcal{F}_i$  corresponding to appropriate subintervals  $I_i \subset I$ .  $\square$

Figure 7 shows an example in which a capsule is swept along a helical path while rotating about  $y$ -axis. The trim curves are elementary.

#### 4. Decomposable sweeps and $\theta$

We now consider sweeps, which though not simple, can be divided into simple sweeps by partitioning the sweep interval. We show that in such sweeps, the trim curves can be obtained by transversal intersection of the contact set with itself, a task which the existing kernels can handle easily. Given an interval  $I$ , we call a partition  $\mathcal{P}$  of  $I$  into consecutive intervals  $I_1, I_2, \dots, I_{k_{\mathcal{P}}}$  to be of width  $\delta$  if  $\max\{\text{length}(I_1), \text{length}(I_2), \dots, \text{length}(I_{k_{\mathcal{P}}})\} = \delta$ .

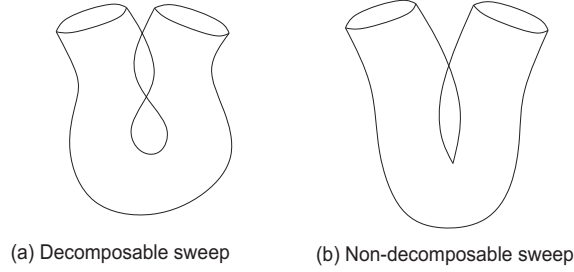


FIGURE 9. Contact-sets of decomposable and non-decomposable sweeps.

DEFINITION 31. We say that the sweep  $(M, h, I)$  is **decomposable** if there exists  $\delta > 0$  such that for all partitions  $\mathcal{P}$  of  $I$  of width  $\delta$ , each sweep  $(M, h, I_i)$  is simple for  $i = 1, \dots, k_{\mathcal{P}}$ . A sweep which is not decomposable is called **non-decomposable**.

Figure 9 schematically illustrates the difference between decomposable and non-decomposable sweeps. The example shown in Figure 7 is of a decomposable sweep in which partitioning the sweep interval  $I$  into 2 equal halves will result in 2 simple sweeps.

PROPOSITION 32. *The sweep  $(M, h, I)$  is decomposable iff  $\mathbf{t-sep} > 0$ . Further, if  $\mathbf{t-sep} > 0$  then all the  $p$ -trim curves are elementary.*

*Proof.* Suppose first that  $\mathbf{t-sep} > 0$ . Let  $\mathcal{P}$  be a partition of  $I$  of width  $\mathbf{t-sep}$ . We show that  $(M, h, I_i)$  is simple for  $i = 1, 2, \dots, k_{\mathcal{P}}$ . Let  $\mathcal{E}_i$  and  $C_{I_i}$  be the envelope and the contact set for  $(M, h, I_i)$  respectively. By Proposition 8, (modulo end-caps),  $\mathcal{E}_i \subset C_{I_i}$ . It needs to be shown that  $C_{I_i} \subset \mathcal{E}_i$ . Suppose not. Let  $y \in C_{I_i}(t)$  such that  $y \notin \mathcal{E}_i$  for some  $t \in I_i$ . Then,  $y \in T_{I_i}$ , i.e.,  $y \in M^o(t')$  for some  $t' \in I_i$ . By an argument similar to that given in Lemma 27 it can be shown that there exists  $\delta t > 0$  such that for all  $t'' \in [t' - \delta t, t' + \delta t]$ ,  $y \in M^o(t'')$ . Let  $y = \sigma(p)$  for  $p = (u, v, t)$ . It follows that  $\ell(p) < \|t - t'\| \leq \text{length}(I_i) \leq \mathbf{t-sep}$ , leading to a contradiction. Hence,  $(M, h, I)$  is decomposable.

Suppose now that  $(M, h, I)$  is decomposable with width-parameter  $\delta$  (cf. Definition 31). Consider a point  $p_0 = (u_0, v_0, t_0) \in \mathcal{F}$  and let  $\sigma(p_0) = y_0$ . Let  $I_1 = [t_0 - \delta, t_0]$  and  $I_2 = [t_0, t_0 + \delta]$ . Further, let  $\mathcal{E}_i$  and  $C_{I_i}$  be the envelope and contact-set for the sweeps  $(M, h, I_i)$  respectively. Observe that  $y_0 \in C_{I_i}$  for  $i = 1, 2$ . Let  ${}_{y_0}\tilde{R}^i = \{(y, x, t) \in C_{I_i} \times M \times I_i \mid y = y_0\}$ . As  $(M, h, I)$  is decomposable with width-parameter  $\delta$ , both  $(M, h, I_1)$  and  $(M, h, I_2)$  are simple, and hence,  $C_{I_i} \subset \mathcal{E}_i$  for  $i = 1, 2$ . Therefore,  $y_0$  belongs to  $\mathcal{E}_1$  and  $\mathcal{E}_2$ . By Lemma 12,  ${}_{y_0}\tilde{R}^1$  and  ${}_{y_0}\tilde{R}^2$  are both singleton sets. Further,  ${}_{y_0}\tilde{R}^1 = {}_{y_0}\tilde{R}^2 = \{(y_0, x, t_0)\}$  for  $x = S(u_0, v_0) \in \partial M$ . Hence,  $\ell(p_0) > \delta$ . Since for all  $p \in \mathcal{F}$ ,  $\ell(p) > \delta$ , we conclude that  $\mathbf{t-sep} \geq \delta > 0$ .

Suppose that  $\mathbf{t-sep} > 0$ . Since  $\ell(p) \geq \mathbf{t-sep}$  for all  $p \in \partial p T_I$  it follows that all the  $p$ -trim curves are elementary.  $\square$

The above proposition provides a *natural* test for decomposability. Further, coupled with Lemma 30, for a decomposable sweep, the problem of excising the trim set can be reduced to transversal intersections. However, note that, the very definition of  $\mathbf{t-sep}$  is *post-facto* as it relies on the trim structures. Besides, it is

the infimum value of the not necessarily continuous function  $\ell$  and is difficult to compute. Thus, the above test of decomposability is not effective.

One of the key contributions of this paper is a novel geometric ‘invariant’ function on the funnel which is computed in closed form and serves the following objectives.

- (1) Quick/efficient and simple detection of decomposability of sweeps, which occur most often in practice.
- (2) Generation of trim curves for non-decomposable sweeps.
- (3) Quantification and detection of singularities on the envelope.

For a point  $p = (u, v, t) \in \mathcal{F}$ , let  $q = \sigma(p)$ . Recall from Section 2.2 that,  $J_\sigma(p) = [\sigma_u \sigma_v \sigma_t]$  is of rank 2. As  $\det(J_\sigma(p)) = 0$ ,  $\{\sigma_u(p), \sigma_v(p), \sigma_t(p)\}$  are linearly dependent. Recall that  $\sigma_t(p) = V(p)$  is the velocity of the point  $S(u, v)$  at time  $t$  (cf. Section 2.2). As  $S$  is regular, the set  $\{\sigma_u(p), \sigma_v(p)\}$  forms a basis for the tangent space to  $\partial M(t)$ . Therefore, we must have  $\sigma_t(p) = n(p) \cdot \sigma_u(p) + m(p) \cdot \sigma_v(p)$  where  $n$  and  $m$  are well-defined (unique) on the funnel and are themselves continuous functions on the funnel.

DEFINITION 33. The function  $\theta : \mathcal{F} \rightarrow \mathbb{R}$  is defined as follows.

$$(3) \quad \theta(p) = n(p) \cdot f_u(p) + m(p) \cdot f_v(p) - f_t(p)$$

where  $f_u, f_v$  and  $f_t$  denote partial derivatives of the function  $f$  w.r.t.  $u, v$  and  $t$  respectively at  $p$ , and  $n$  and  $m$  are as defined above.

Note that, unlike  $\ell$ ,  $\theta$  is easily and robustly computable continuous function on the funnel. Now we are ready to state one of the main theorems of this paper.

THEOREM 34. *If for all  $p \in \mathcal{F}$ ,  $\theta(p) > 0$ , then the sweep is decomposable. Further, if there exists  $p \in \mathcal{F}$  such that  $\theta(p) < 0$ , then the sweep is non-decomposable.*

The proof is given in Section 5.6 which highlights many other surprisingly strong properties of the function  $\theta$ .

DEFINITION 35. The function  $\theta$  partitions the funnel  $\mathcal{F}$  into three sets, viz. (i)  $\mathcal{F}^+ := \{p \in \mathcal{F} | \theta(p) > 0\}$ , (ii)  $\mathcal{F}^- := \{p \in \mathcal{F} | \theta(p) < 0\}$  and (iii)  $\mathcal{F}^0 := \{p \in \mathcal{F} | \theta(p) = 0\}$ . Further, we define  $C_I^+ := \sigma(\mathcal{F}^+)$ ,  $C_I^- := \sigma(\mathcal{F}^-)$  and  $C_I^0 := \sigma(\mathcal{F}^0)$ .

Figure 10 schematically illustrates the sets  $\mathcal{F}^+, \mathcal{F}^-$  and  $\mathcal{F}^0$  on the funnel and sets  $C_I^-, C_I^+$  and  $C_I^0$  on the contact set.

Note that, for  $(M, h, I)$  in general position, either  $\mathcal{F}^-$  is a non-empty open set or  $\mathcal{F} = \mathcal{F}^+$ . Whence, the above theorem provides an efficient ‘open’ test for decomposability, namely, a sweep  $(M, h, I)$  is decomposable iff the open set  $\mathcal{F}^-$  is empty. By continuity of the function  $\theta$ , the set  $\mathcal{F}^-$  is empty iff the set  $\mathcal{F}^0$  is empty. Since  $\mathcal{F}$  is a smooth manifold, every point of  $\mathcal{F}$  is accessible via the procedural parametrization discussed in Appendix C. Most kernels will have an effective procedure for computing the set  $\mathcal{F}^0$  provided  $\nabla\theta$  is non-zero on the curve  $\mathcal{F}^0$ . This is demonstrated in Section 5.3. Thus, all components of  $\mathcal{F}^0$  will be discovered for the same reason that most kernels discover all the intersections of two given solids.

## 5. Properties of the invariant $\theta$

In this section we prove some key properties of  $\theta$ , namely, its invariance under the re-parametrization of the surface being swept and its relation with the notion

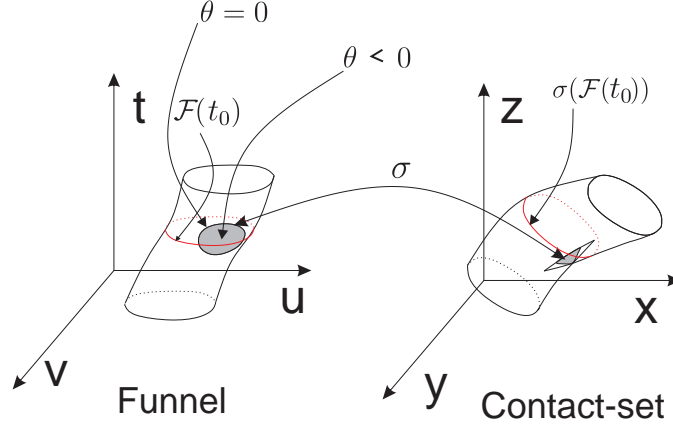


FIGURE 10. The shaded region on  $\mathcal{F}$  and  $C_I$  corresponds to  $\mathcal{F}^-$  and  $C_I^-$  respectively. A curve of contact is shown in red.

of inverse trajectory used in earlier works. Finally, we use these properties along with Proposition 32, to prove Theorem 34.

**5.1. Invariance of  $\theta$ .** We show that the function  $\theta$  is invariant of the parametrization of  $\partial M$  and hence, intrinsic to the sweep.

**THEOREM 36.** *If  $\bar{S}$  is a re-parametrization of the surface  $S$  so that  $q := \bar{S}(\bar{u}, \bar{v}) = S(u, v)$ , and if  $g(q, t) = 0$ , then  $\theta(u, v, t) = \bar{\theta}(\bar{u}, \bar{v}, t)$ .*

*Proof.* Suppose as before that the boundary  $\partial M$  is specified by the parametrized surface  $S$ . Let  $\phi : \mathbb{R}^2 \rightarrow \mathbb{R}^2$  be a re-parametrization map of  $S$  and  $\bar{S} := S \circ \phi$ . Since  $\phi$  is a diffeomorphism,  $d\phi$  is an isomorphism at every point in the entire domain of  $\phi$ . Let  $\phi(\bar{u}, \bar{v}) = (u(\bar{u}, \bar{v}), v(\bar{u}, \bar{v}))$ . For convenience of expression, we extend  $\phi$  to define it on the parameter space of the sweep map  $\sigma$  so that  $\phi(\bar{u}, \bar{v}, t) = (u, v, t)$ . Hence the re-parametrized sweep map (for  $\bar{S}$ ) is simply  $\bar{\sigma} = \sigma \circ \phi$ . Recall that  $f(u, v, t) = \langle \hat{N}(u, v, t), V(u, v, t) \rangle$ , where  $\hat{N}(u, v, t)$  is the unit outward normal to  $\partial M(t)$  at the point  $A(t) \cdot S(u, v) + b(t)$ . It is easy to check that  $\hat{N}(u, v, t)$  can also be expressed as  $A(t) \cdot (\mathcal{G} \circ S)(u, v)$ , where  $\mathcal{G} : \partial M \rightarrow S^2$  is the intrinsic Gauss map,  $S^2$  being the unit sphere and  $\circ$  stands for the usual composition of functions. Thus,

$$f(u, v, t) = \langle \hat{N}(u, v, t), V(u, v, t) \rangle = \langle A(t) \cdot (\mathcal{G} \circ S)(u, v), V(u, v, t) \rangle$$

Similarly, computing with the re-parametrization  $\bar{S}$ , and using the fact that  $\bar{S} = S \circ \phi$ , we have  $\bar{f} = f \circ \phi$ . Differentiating w.r.t.  $\bar{u}, \bar{v}$  and  $t$  we get  $\nabla \bar{f} = d\phi^T \cdot \nabla f$  where  $d\phi$  is the Jacobian of the map  $\phi$ .

Observe that, from Eq. 3, for  $\bar{p} = (\bar{u}, \bar{v}, t)$  and  $p = \phi(\bar{p}) = (u, v, t)$ ,  $\theta(p) = \langle \nabla f(p), z \rangle$  where  $z = (n, m, -1)$  spans the null-space of  $J_\sigma|_p$  for  $p \in \mathcal{F}$ . In order to compute  $\bar{z}$  for the re-parametrized sweep we see that  $J_{\bar{\sigma}} = J_\sigma \circ d\phi$  and  $\bar{z} = d\phi^{-1}z$ . Now using  $\nabla \bar{f} = d\phi^T \cdot \nabla f$ , we get that

$$\bar{\theta}(\bar{p}) = \langle \nabla \bar{f}(\bar{p}), \bar{z} \rangle = \langle d\phi^T \cdot \nabla f(p), d\phi^{-1} \cdot z \rangle = \langle \nabla f(p), z \rangle = \theta(p)$$

This proves the theorem.  $\square$

**5.2. Geometric meaning of  $\theta$ .** For a smooth point  $w$  of  $W$ , let  $\mathcal{T}_W(w)$  denote the tangent space to  $W$  at  $w$ .

We show that the function  $\theta$  arises out of the relation between two 2-frames on  $\mathcal{T}_{C_I}$ . Let  $p = (u, v, t) \in \mathcal{F}$  be such that  $\sigma(p)$  is a smooth point of  $C_I$ . We first compute a natural 2-frame  $\mathcal{X}(p)$  in  $\mathcal{T}_{\mathcal{F}}(p)$ . Note that,  $\mathcal{F}$  being the zero level-set of the function  $f$ ,  $\nabla f|_p \perp \mathcal{T}_{\mathcal{F}}(p)$ . We set  $\beta := (-f_v, f_u, 0)$  and note that  $\beta \perp \nabla f$ . It is easy to see that  $\beta$  is tangent to the p-curve-of-contact  $\mathcal{F}(t)$ . Let  $\alpha := \nabla f \times \beta = (-f_u f_t, -f_v f_t, f_u^2 + f_v^2)$ . Here  $\times$  is the cross-product in  $\mathbb{R}^3$ . Clearly, the set  $\{\alpha, \beta\}$  forms a basis of  $\mathcal{T}_{\mathcal{F}}(p)$  if  $(f_u, f_v) \neq (0, 0)$ . Since  $\nabla f \neq 0$ , if  $(f_u, f_v) = (0, 0)$  then  $f_t \neq 0$  and  $\{\alpha', \beta'\} := \{(1, 0, 0), (0, f_t, 0)\}$  serves as a basis for  $\mathcal{T}_{\mathcal{F}}(p)$ . Figure 2 illustrates the basis  $\{\alpha, \beta\}$  schematically.

The set  $\{J_\sigma \cdot \alpha, J_\sigma \cdot \beta\} \subseteq \mathcal{T}_{C_I}(\sigma(p))$  and can be expressed in terms of  $\{\sigma_u, \sigma_v\}$  as follows

$$[J_\sigma \cdot \alpha \quad J_\sigma \cdot \beta] = [\sigma_u \quad \sigma_v] \underbrace{\begin{bmatrix} -f_t \cdot f_u + n \cdot (f_u^2 + f_v^2) & -f_v \\ -f_t \cdot f_v + m \cdot (f_u^2 + f_v^2) & f_u \end{bmatrix}}_{\mathcal{D}(p)}$$

Note that,

$$(4) \quad \det(\mathcal{D}(p)) = (f_u^2 + f_v^2)(n \cdot f_u + m \cdot f_v - f_t)$$

$$(5) \quad = (f_u^2 + f_v^2)\theta(p)$$

Clearly, if  $(f_u, f_v) \neq (0, 0)$  then  $\det(\mathcal{D}(p))$  is a positive scalar multiple of  $\theta(p)$ . Again, if  $(f_u, f_v) = (0, 0)$ , expressing  $\{J_\sigma \cdot \alpha', J_\sigma \cdot \beta'\}$  in terms of  $\{\sigma_u, \sigma_v\}$  we see that  $\det(\mathcal{D}(p)) = \theta(p) = -f_t$ .

The above relation between  $\{\sigma_u, \sigma_v\}$  and  $\{J_\sigma \cdot \alpha, J_\sigma \cdot \beta\}$  shows that if  $\theta(p) \neq 0$ ,  $\mathcal{T}_{C_I}(y)$  and  $\mathcal{T}_{\partial M(t)}(y)$  are identical (as subspaces of  $\mathbb{R}^3$ ) for  $y = \sigma(p)$ , i.e.,  $\partial M(t)$  makes tangential contact with  $C_I$  at  $y$ .

**5.3. Non-singularity of  $\theta$ .** We give a sweep example which will demonstrate the non-singularity of the function  $\theta$ . We show that on the set  $\mathcal{F}^0$ ,  $\nabla \theta \neq \bar{0}$ . Consider a sphere parametrized as  $S(u, v) = (\cos v \cos u, \cos v \sin u, \sin v)$ ,  $v \in [-\frac{\pi}{2}, \frac{\pi}{2}]$ ,  $u \in [-\pi, \pi]$  swept along a curvilinear trajectory given by  $h(t) = (A(t), b(t))$ ,  $A(t) = I$ ,  $b(t) = (\frac{1}{2} \cos 2t, \frac{1}{2} \sin 2t, 0)$ ,  $t \in [0, 1]$ . The unit outward normal at  $S(u, v)$  at time  $t$  is given by  $\hat{N}(u, v, t) = (\cos v \cos u, \cos v \sin u, \sin v)$  and velocity is given by  $V(u, v, t) = (-\sin 2t, \cos 2t, 0)$ . The envelope function is  $f(u, v, t) = \langle \hat{N}(u, v, t), V(u, v, t) \rangle = \cos v \sin(u - 2t)$ . The funnel  $\mathcal{F}$  is given by (i)  $u = 2t - \pi$ ,  $v \in [-\frac{\pi}{2}, \frac{\pi}{2}]$  and (ii)  $u = 2t$ ,  $v \in [-\frac{\pi}{2}, \frac{\pi}{2}]$ . Hence,  $u$  and  $v$  can serve as local parameters of  $\mathcal{F}$ . In component (ii) of the funnel, we see that  $\theta > 0$ , hence we will only consider component (i). On  $\mathcal{F}$ ,  $\sigma_t = n \cdot \sigma_u + m \cdot \sigma_v$  where  $n = \frac{-1}{\cos v}$  and  $m = 0$ , whence,  $\theta(u, v, t) = n \cdot f_u + m \cdot f_v - f_t = 2 \cos v - 1$ . The set  $\mathcal{F}^0$  is given by  $v = \pm \frac{\pi}{3}$ ,  $u = 2t - \pi$ . On  $\mathcal{F}^0$ ,  $\frac{\partial \theta}{\partial u} = 0$  and  $\frac{\partial \theta}{\partial v} = 2 \sin v \neq 0$ .

An important consequence of non-singularity of  $\theta$  is that its zero set, i.e.,  $\mathcal{F}^0$  can be computed robustly and easily.

**5.4. Singularities and their detection on the envelope.** Now we characterize the cusp-singular points of  $C_I$ . Geometrically, these are precisely the points where  $C_I$  intersects itself non-transversally. At such points, the dimension of  $\mathcal{T}_{C_I}$

drops below 2. Identification of such points is important because any parametrization of  $C_I$  will be degenerate in the neighborhood of such points. Toward this, consider the following restriction of  $\sigma$  to the funnel:  $\sigma|_{\mathcal{F}} : \mathcal{F} \rightarrow \mathbb{R}^3$ . Note that  $\sigma|_{\mathcal{F}}(\mathcal{F}) = C_I$ .

**DEFINITION 37.** The set  $C_I$  is said to have a **cuspidal singularity** at a point  $\sigma(p) = x \in C_I$  if  $\sigma|_{\mathcal{F}}$  fails to be an immersion at  $p$ .

A basic result about immersion (see [5]) implies that if  $\sigma|_{\mathcal{F}}$  is an immersion at a point  $p$ , then there is a neighborhood  $\mathcal{N}$  of  $p$  such that  $\sigma|_{\mathcal{F}}$  is a local diffeomorphism from  $\mathcal{N}$  onto its image.

**LEMMA 38.** *Let  $p_0 \in \mathcal{F}$  and  $\sigma(p_0) = x_0$ . The point  $x_0$  is a cuspidal singularity iff  $\theta(p_0) = 0$ .*

*Proof.* From subsection 5.2,  $\theta(p_0)$  is a positive multiple of the determinant relating frames  $\{\sigma_u, \sigma_v\}$  and  $\{J_\sigma \cdot \alpha, J_\sigma \cdot \beta\}$  at  $x_0$ . Since the set  $\{\sigma_u, \sigma_v\}$  is always linearly independent, it follows that  $\{J_\sigma \cdot \alpha, J_\sigma \cdot \beta\}$  is linearly dependent iff  $\sigma|_{\mathcal{F}}$  fails to be an immersion at  $p_0$  iff  $\theta(p_0) = 0$ .  $\square$

In other words, the set  $C_I^0$  is the set of cuspidal singular points in  $C_I$ .

**5.5. Relation with inverse trajectory.** We now show the relation of the function  $\theta$  with inverse trajectory [4, 7] used by previous authors. Given a trajectory  $h$  and a fixed point  $x$  in object-space, the inverse trajectory of  $x$  is the set of points in the object-space which get mapped to  $x$  at some time instant by  $h$ , i.e.  $\{z \in \mathbb{R}^3 | \exists t \in [0, 1], A(t) \cdot z + b(t) = x\}$ .

**DEFINITION 39.** Given a trajectory  $h$ , the **inverse trajectory**  $\bar{h}$  is defined as the map  $\bar{h} : I \rightarrow (SO(3), \mathbb{R}^3)$  given by  $\bar{h}(t) = (A^t(t), -A^t(t) \cdot b(t))$ . Thus, for a fixed point  $x \in \mathbb{R}^3$ , the inverse trajectory of  $x$  is the map  $\bar{y} : I \rightarrow \mathbb{R}^3$  given by  $\bar{y}(t) = A^t(t) \cdot (x - b(t))$ .

The range of  $\bar{y}$  is  $\{A^t(t) \cdot x - A^t(t) \cdot b(t) | t \in I\}$ . We list some facts about  $\bar{y}$  in Appendix B which will be used in proving Theorem 40.

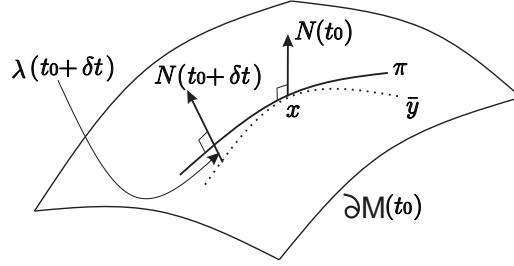
For the inverse trajectory  $\bar{y}$  of a point  $x \in \partial M(t_0)$ , let  $\pi$  be the projection of  $\bar{y}$  on  $\partial M(t_0)$ . Let  $\lambda(t)$  be the signed distance of  $\bar{y}(t)$  from  $\partial M(t_0)$ . If the point  $\bar{y}(t)$  is in  $M^o(t_0)$ ,  $Ext(M(t_0))$  (the exterior of  $M$ ) or on the surface  $\partial M(t_0)$ , then  $\lambda(t)$  is negative, positive or zero respectively. Then we have  $\bar{y}(t) - \pi(t) = \lambda(t)N(t)$ , where  $\pi(t)$  is the projection of  $\bar{y}(t)$  on  $\partial M(t_0)$  along the unit outward pointing normal  $N(t)$  to  $\partial M(t_0)$  at  $\pi(t)$ . This is illustrated in Figure 11. So, the following relation holds for  $\lambda$ .

$$(6) \quad \lambda(t) = \langle \bar{y}(t) - \pi(t), N(t) \rangle$$

**THEOREM 40.** *For  $p = (u_0, v_0, t_0) \in \mathcal{F}$ ,*

$$\theta(p) = \ddot{\lambda}(t_0) = \left\langle -\ddot{\sigma} + 2\dot{A} \cdot V, N \right\rangle + \kappa v^2$$

where  $\ddot{\cdot}$  denotes the second derivative of  $\lambda$ ,  $\kappa$  is the normal curvature of  $S$  at  $(u_0, v_0)$  along velocity  $V(p)$ ,  $N$  is the unit outward normal to  $S$  at  $(u_0, v_0)$  and  $v^2 = \langle V(p), V(p) \rangle$ .

FIGURE 11. The inverse trajectory of  $x$  intersects  $M^o(t_0)$ .

*Proof.* Differentiating Eq. 6 with respect to time and denoting derivative w.r.t.  $t$  by  $\dot{\phantom{x}}$ , we get

$$(7) \quad \dot{\lambda}(t) = \langle \dot{\bar{y}}(t) - \dot{\pi}(t), N(t) \rangle + \langle \bar{y}(t) - \pi(t), \dot{N}(t) \rangle$$

$$(8) \quad \ddot{\lambda}(t) = \langle \ddot{\bar{y}}(t) - \ddot{\pi}(t), N(t) \rangle + 2 \langle \dot{\bar{y}}(t) - \dot{\pi}(t), \dot{N}(t) \rangle + \langle \bar{y}(t) - \pi(t), \ddot{N}(t) \rangle$$

At  $t = t_0$ ,  $\bar{y}(t_0) = \pi(t_0)$ . Since  $\dot{y}(t_0) = V(p) \perp N(p)$ , it follows from Eq. 18 that  $\dot{\bar{y}}(t_0) \perp N(p)$ . It is easy to verify that  $\dot{\pi}(t_0) = \dot{\bar{y}}(t_0)$ . Hence,

$$(9) \quad \lambda(t_0) = \dot{\lambda}(t_0) = 0$$

From Eq. 8 and Eq. 20 it follows that

$$(10) \quad \begin{aligned} \ddot{\lambda}(t_0) &= \langle \ddot{\bar{y}}(t_0) - \ddot{\pi}(t_0), N(t_0) \rangle \\ &= \langle -\ddot{y}(t_0) + 2\dot{A}(t_0) \cdot \dot{y}(t_0) - \ddot{\pi}(t_0), N(t_0) \rangle \end{aligned}$$

Since  $\pi(t) \in S(t_0)$  for all  $t$  in some neighbourhood  $U$  of  $t_0$ , we have that  $\langle \dot{\pi}(t), N(t) \rangle = 0, \forall t \in U$ . Hence  $\langle \ddot{\pi}(t), N(t) \rangle + \langle \dot{\pi}(t), \dot{N}(t) \rangle = 0, \forall t \in U$ . Hence  $-\langle \ddot{\pi}(t_0), N(t_0) \rangle = \langle \dot{\pi}(t_0), \dot{N}(t_0) \rangle = \langle \dot{\pi}(t_0), \mathcal{G}^*(\dot{\pi}(t_0)) \rangle = \langle \dot{y}(t_0), \mathcal{G}^*(\dot{y}(t_0)) \rangle = \langle V(p), \mathcal{G}^*(V(p)) \rangle = \kappa v^2$ . Here  $\mathcal{G}^*$  is the differential of the Gauss map, i.e. the curvature tensor of  $S(t_0)$  at point  $x$ . Using this in Eq. 10 and the fact that  $\dot{y}(t_0) = \dot{\sigma}(p)$ ,  $\ddot{y}(t_0) = \ddot{\sigma}(p)$  we get

$$(11) \quad \ddot{\lambda}(t_0) = \langle -\ddot{\sigma}(p) + 2\dot{A}(t_0) \cdot V(p), N(t_0) \rangle + \kappa v^2$$

Recalling definition of  $\theta(p)$  from Eq. 3

$$lf_u + mf_v - f_t = \langle l\hat{N}_u + m\hat{N}_v, V \rangle + \langle \hat{N}, lV_u + mV_v \rangle - \langle \hat{N}_t, V \rangle - \langle \hat{N}, V_t \rangle$$

Here  $\hat{N}_u = \mathcal{G}^*(\sigma_u)$  and  $\hat{N}_v = \mathcal{G}^*(\sigma_v)$  where  $\mathcal{G}^*$  is the shape operator (differential of the Gauss map) of  $S(t_0)$  at  $(u_0, v_0)$ . Also,  $V_u = A_t \cdot S_u$  and  $V_v = A_t \cdot S_v$ . Assume without loss of generality that  $A(t_0) = I$  and  $b(t_0) = 0$ , hence  $\hat{N} = A(t_0) \cdot N = N$ ,  $\sigma_u = S_u$  and  $\sigma_v = S_v$ . Using Eq. 16 and the fact that  $V = \sigma_t = l\sigma_u + m\sigma_v$  we get

$$(12) \quad \begin{aligned} lf_u + mf_v - f_t &= \langle \mathcal{G}^* \cdot V, V \rangle + 2 \langle A_t \cdot V, N \rangle - \langle V_t, N \rangle \\ &= \kappa v^2 + \langle 2A_t \cdot V - V_t, N \rangle \end{aligned}$$

From Eqs. 11 and 12 and the fact that  $\frac{\partial \sigma}{\partial t^2} = V_t$  we get  $\theta(p) = lf_u + mf_v - f_t = \ddot{\lambda}(t_0)$ .

□

From Theorem 40 it is clear that the function  $\theta$  is intimately connected with the curvature of the solid and that of the trajectory. Further, unlike in the approaches in [4] and [7] in which every sampled point of  $C_I$  must be subjected to the inverse trajectory test in order to perform trimming, we show in the following section that ultimately only a few points of  $\mathcal{F}^0$  are used for computing the trim curves. Hence, the trim set  $T_I$ , including the region  $\mathcal{F}^-$ , need not be explored at all.

We now give the proof of Theorem 34 which gives an efficient test for decomposability using the function  $\theta$ .

**5.6. Proof of Theorem 34.** **Theorem 34** *If for all  $p \in \mathcal{F}$ ,  $\theta(p) > 0$ , then the sweep is decomposable. Further, if there exists  $p \in \mathcal{F}$  such that  $\theta(p) < 0$ , then the sweep is non-decomposable.*

*Proof.* Suppose that for all  $p \in \mathcal{F}$ ,  $\theta(p) > 0$ . For  $p \in \mathcal{F}$ , let  $t(p)$  denote the  $t$ -coordinate of  $p$ . Consider the set of points  $P = \{p \in \mathcal{F} | \exists p' \in \mathcal{F}, p' \neq p, \sigma(p) = \sigma(p') \text{ and } \sigma^{-1}(\sigma(p)) = \{p, p'\}\}$ . Note that, by the general position assumption, there are only finitely many points  $p \in \mathcal{F}$  such that  $\sigma^{-1}(\sigma(p))$  is of cardinality greater than two. Hence such points may be ignored in the following discussion. By the general position assumption,  $P$  is a collection of smooth curves in  $\mathcal{F}$ . For  $p \in P$ , let  $p'$  denote the unique point in  $P$  such that  $p \neq p'$  and  $\sigma(p) = \sigma(p')$ . Further, we define  $\delta(p) = \|t(p) - t(p')\|$ . Let  $\delta := \inf_{p \in P} \delta(p)$ . Consider two cases as follows:

**Case (i):**  $\delta = 0$ , i.e., there exists a sequence  $(p_n)$  in a curve  $C$  of  $P$  such that  $\lim_{n \rightarrow \infty} \delta(p_n) = 0$ . Hence there exists  $p_0 \in \bar{C}$  (closure of  $C$ ) which is a limit point of  $(p_n)$ . Since  $\lim_{n \rightarrow \infty} \delta(p_n) = \lim_{n \rightarrow \infty} \|t(p_n) - t(p'_n)\| = 0$  and  $\partial M$  is free from self-intersections, we have that  $\lim_{n \rightarrow \infty} \|p_n - p'_n\| = 0$ . Hence, for a small neighborhood  $\mathcal{N}$  of  $p_0$  in  $\mathcal{F}$ , we may parametrize the smooth curve  $\bar{C} \cap \mathcal{N}$  by a map  $\gamma$  so that  $\gamma(0) = p_0$  and, for  $s \neq 0$ ,  $\gamma(s), \gamma(-s) \in C \cap \mathcal{N}$  and  $\sigma(\gamma(s)) = \sigma(\gamma(-s))$ . Let  $\Gamma(s) := \sigma(\gamma(s))$ . Note that  $\Gamma(s) = \Gamma(-s)$ . Now,

$$\begin{aligned} \frac{d\Gamma}{ds} \Big|_0 &= \lim_{\Delta s \rightarrow 0} \frac{\Gamma(\Delta s) - \Gamma(0)}{\Delta s} = \lim_{\Delta s \rightarrow 0} \frac{\Gamma(0) - \Gamma(-\Delta s)}{\Delta s} \\ &= \lim_{\Delta s \rightarrow 0} \frac{\Gamma(0) - \Gamma(\Delta s)}{\Delta s} = - \lim_{\Delta s \rightarrow 0} \frac{\Gamma(\Delta s) - \Gamma(0)}{\Delta s} \end{aligned}$$

Hence,

$$\frac{d\Gamma}{ds} \Big|_0 = J_{\sigma|_{\gamma(0)}} \cdot \frac{d\gamma}{ds} \Big|_0 = 0$$

Since  $\frac{d\gamma}{ds} \Big|_0 \in \mathcal{T}_{\mathcal{F}}(p_0)$ , the map  $\sigma|_{\mathcal{F}} : \mathcal{F} \rightarrow C_I$  fails to be an immersion at  $p_0$  and by Lemma 38 we get that  $\theta(p_0) = 0$ , which is a contradiction to the hypothesis.

**Case (ii):**  $\delta > 0$ . Let  $\{I_1, I_2, \dots, I_k\}$  be a partition of  $I$  of width  $\frac{\delta}{2}$ . Let  $\mathcal{F}_i$  and  $\mathcal{C}_{I_i}$  denote the funnel and the contact set corresponding to subinterval  $I_i$ . Then it is clear that for each  $i$ ,  $\sigma : \mathcal{F}_i \rightarrow \mathcal{C}_{I_i}$  is a diffeomorphism, i.e., for each  $i$ ,  $\mathcal{C}_{I_i}(t) \cap \mathcal{C}_{I_i}(t') = \emptyset$  for all  $t, t' \in I_i$ ,  $t \neq t'$ . We show that the subproblems  $(M, h, I_i)$  are simple for all  $i$ . Suppose not, i.e., for some  $i$ , there exists  $t \in I_i$  such that  $\mathcal{C}_{I_i}(t) \cap M^o(t') \neq \emptyset$  for some  $t' \in I_i$ . Hence the trim set  $T_{I_i}$  is not empty. By Lemma 30, for all but finitely many points in  $\partial T_{I_i}$  there are two points  $p_1, p_2 \in \partial p T_{I_i}$  such that  $\sigma(p_1) = \sigma(p_2) = y$ . If  $p_1 \in \mathcal{F}_i(t_1)$  and  $p_2 \in \mathcal{F}_i(t_2)$  then it follows that  $\mathcal{C}_{I_i}(t_1) \cap \mathcal{C}_{I_i}(t_2) = y$  leading to contradiction. Hence, the subproblems  $(M, h, I_i)$

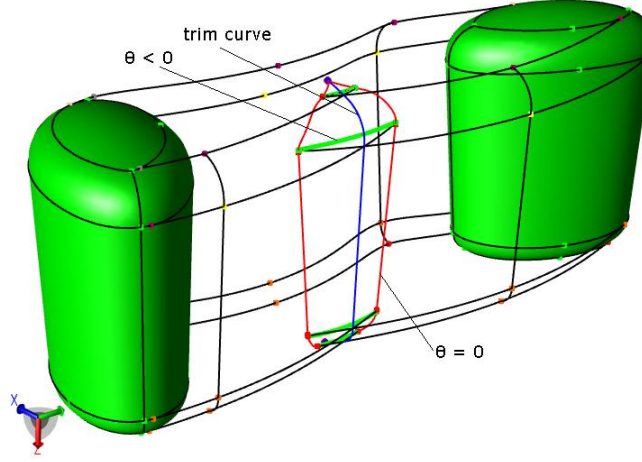


FIGURE 12. Example of a non-decomposable sweep: an elliptical cylinder being swept along  $y$ -axis while undergoing rotation about  $z$ -axis. The curve  $\theta = 0$  is shown in red and trim curve is shown in blue. The portion of the swept edges where  $\theta$  is negative is shown in green.

are simple for all  $i$ . It follows that  $(M, h, I)$  is decomposable with width-parameter  $\frac{\delta}{2}$ .

Hence we have proved that if for all  $p \in \mathcal{F}$ ,  $\theta(p) > 0$  then the sweep is decomposable.

Suppose now that there exists  $p = (u, v, t) \in \mathcal{F}$  such that  $\theta(p) < 0$ . Let  $y = \sigma(p)$ . Recall the definition of the function  $\lambda$  from Equation 6 and relation  $\theta(p) = \ddot{\lambda}(t)$  from Theorem 40. Clearly, if  $\ddot{\lambda}(t) < 0$ , then  $t$  is a local maxima of the function  $\lambda$  and the inverse trajectory of  $y$  intersects  $M^o(t)$ . So, there exists  $\epsilon > 0$  such that for all  $\delta \in (0, \epsilon)$ , there exists  $w_\delta \in M^o(t)$  such that  $A(t+\delta) \cdot w_\delta + b(t+\delta) = y$ . Hence, the interval  $[t, t + \delta] \subset L(p)$ . Thus  $\ell(p) = 0$  and hence  $\mathbf{t-sep} = 0$ . By Proposition 32, the sweep is non-decomposable.  $\square$

## 6. Trimming non-decomposable sweeps using $\theta$

In this section we look at singular p-trim curves, i.e., a curve  $C$  of  $\partial pT_I$  where  $\inf_{p \in C} \ell(p) = 0$ . We show that  $C_I^- \subset T_I$  and that  $C_I^0$  makes contact with  $\partial T_I$ , thereby providing a seed for tracing  $\partial T_I$ . Figure 18(b) schematically illustrates singular p-trim curves. Figures 12, 13, 14, 15, 16 and 17 show six examples of non-decomposable sweeps and the associated singular trim curves. In Figures 12, 13, 14 and 15 the 1-cage of the envelope, i.e., the swept edges are shown with the portion where  $\theta > 0$  shown in black and the portion where  $\theta < 0$  shown in green. The curve  $C_I^0$  is shown in red and the trim curve  $\partial T_I$  is shown in blue.

In Figures 16(a) and 17(a), curves of contact at a few time instances are shown. The portions of  $C_I(t)$  where  $\theta > 0$  and  $\theta < 0$  on  $\mathcal{F}(t)$  are shown in black and green respectively. In Figures 16(b) and 17(b) the portion where  $\theta$  is negative is excised, the curve  $C_I^0$  is shown in red and the trim curve  $\partial T_I$  is shown in blue. Note that

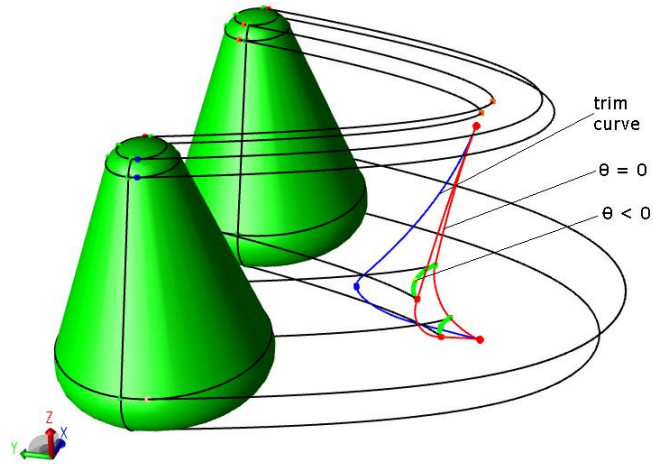


FIGURE 13. Example of a non-decomposable sweep: a cone being swept along a parabola. The curve  $\theta = 0$  is shown in red and trim curve is shown in blue. The portion of the swept edges where  $\theta$  is negative is shown in green.

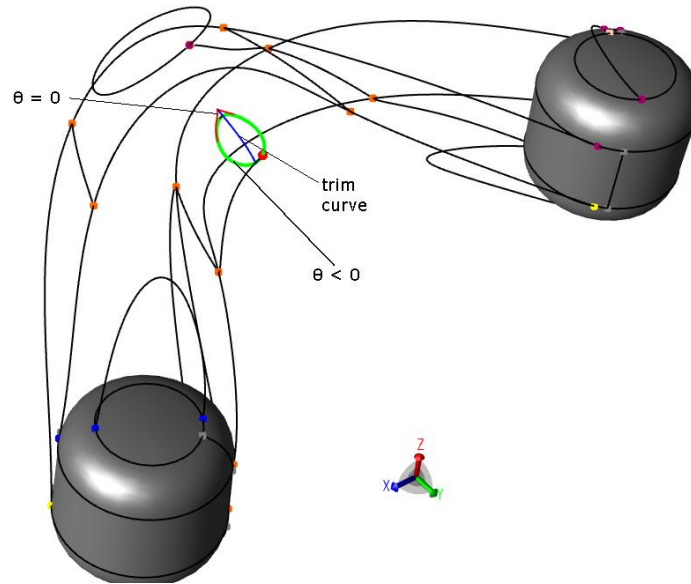


FIGURE 14. Example of a non-decomposable sweep: a cylinder being swept along a cosine curve in  $xy$ -plane while undergoing rotation about  $x$ -axis. The curve  $\theta = 0$  is shown in red and trim curve is shown in blue. The portion of the swept edges where  $\theta$  is negative is shown in green.

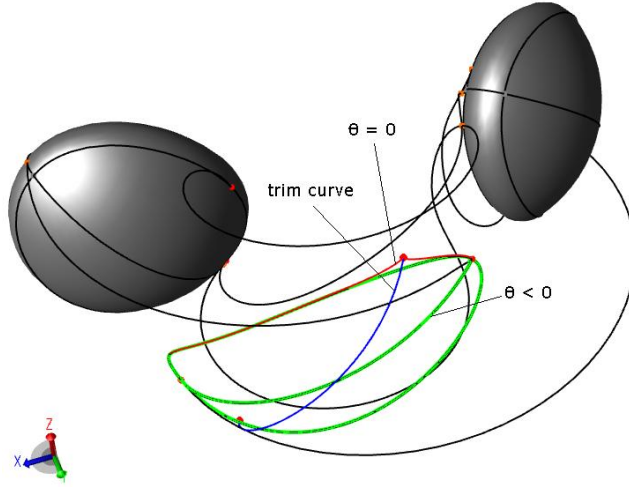


FIGURE 15. Example of a non-decomposable sweep: a blended intersection of a sphere and an ellipsoid being swept along a circular arc in  $xy$ -plane while undergoing rotation about  $z$ -axis. The curve  $\theta = 0$  is shown in red and trim curve is shown in blue. The portion of the swept edges where  $\theta$  is negative is shown in green.

$C_I^0$  and  $\partial T_I$  make contact, as we explain in this section. Figure 19 schematically illustrates the interaction between curves of contact in non-decomposable sweeps.

**PROPOSITION 41.** *If  $C$  is a singular  $p$ -trim curve and  $p_0 \in C$  is a limit-point of  $(p_n) \subset C$  such that  $\lim_{n \rightarrow \infty} \ell(p_n) = 0$ , then  $\theta(p_0) = 0$ .*

*Proof.* For  $p \in \mathcal{F}$ , let  $t(p)$  denote the  $t$ -coordinate of  $p$ . By Lemma 27 it follows that for each  $p_n \in (p_n)$  there exists  $p'_n \in C$  such that  $\sigma(p_n) = \sigma(p'_n)$ . Since  $\lim_{n \rightarrow \infty} \|t(p_n) - t(p'_n)\| = 0$  and  $\partial M$  is free from self-intersections, we have that  $\lim_{n \rightarrow \infty} \|p_n - p'_n\| = 0$ . Hence, for a small neighborhood  $\mathcal{N}$  of  $p_0$  in  $\mathcal{F}$ , we may parametrize  $C \cap \mathcal{N}$  by a map  $\gamma$  so that  $\gamma(0) = p_0$  and, for  $s \neq 0$ ,  $\gamma(s), \gamma(-s) \in \mathcal{N} \cap C$  and  $\sigma(\gamma(-s)) = \sigma(\gamma(s))$ . Let  $\Gamma(s) := \sigma(\gamma(s))$ . Then,

$$\begin{aligned} \frac{d\Gamma}{ds} \Big|_0 &= \lim_{\Delta s \rightarrow 0} \frac{\Gamma(\Delta s) - \Gamma(0)}{\Delta s} = \lim_{\Delta s \rightarrow 0} \frac{\Gamma(0) - \Gamma(-\Delta s)}{\Delta s} \\ &= \lim_{\Delta s \rightarrow 0} \frac{\Gamma(0) - \Gamma(\Delta s)}{\Delta s} = - \lim_{\Delta s \rightarrow 0} \frac{\Gamma(\Delta s) - \Gamma(0)}{\Delta s} \end{aligned}$$

Hence,

$$\frac{d\Gamma}{ds} \Big|_0 = J_\sigma|_{\gamma(0)} \cdot \frac{d\gamma}{ds} \Big|_0 = 0$$

Since  $\frac{d\gamma}{ds} \Big|_0 \in \mathcal{T}_{\mathcal{F}}(p_0)$ , the map  $\sigma|_{\mathcal{F}} : \mathcal{F} \rightarrow C_I$  fails to be an immersion at  $p_0$  and by Lemma 38 we conclude that  $\theta(p_0) = 0$ .  $\square$

**DEFINITION 42.** A limit point  $p$  of a singular  $p$ -trim curve  $C$  such that  $\theta(p) = 0$  will be called a **singular trim point**.

In Figure 18(b) a singular trim point  $p_0$  is shown on  $\partial p T_I$ .

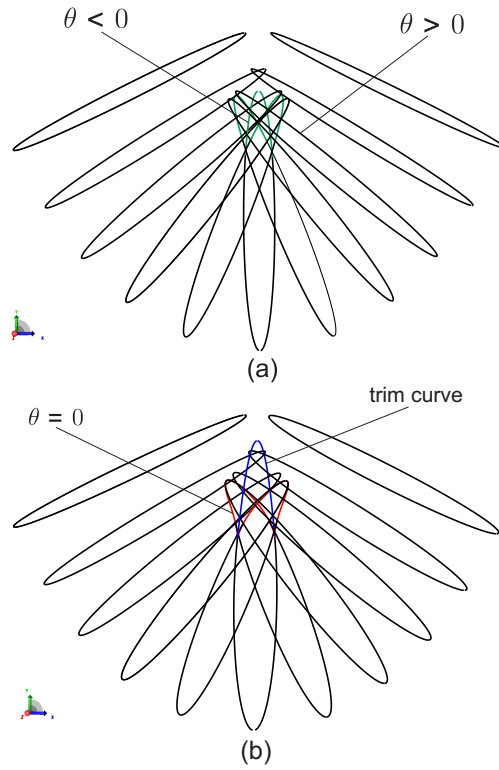


FIGURE 16. Example of a non-decomposable sweep: a sphere being swept along a parabola (a) Curves of contact at a few time instances (b) The curve  $\theta = 0$  is shown in red and trim curve is shown in blue.

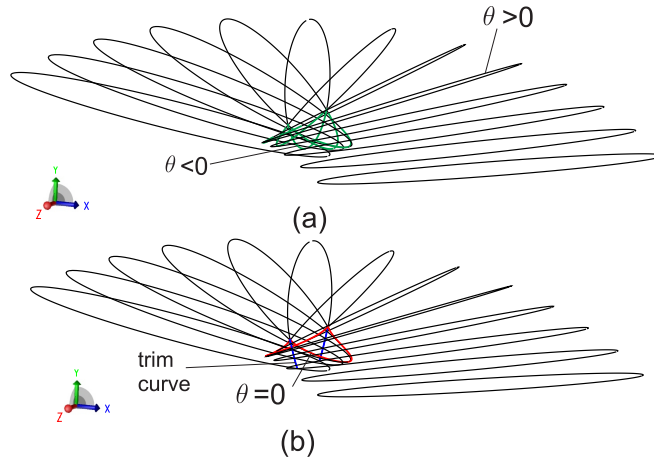


FIGURE 17. Example of a non-decomposable sweep: an ellipsoid being swept along a circular arc (a) Curves of contact at a few time instances (b) The curve  $\theta = 0$  is shown in red and trim curve is shown in blue.

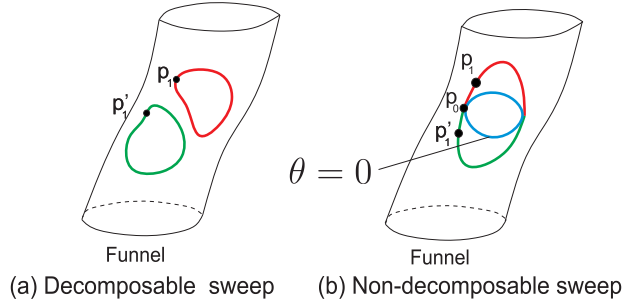


FIGURE 18. The  $p$ -trim curves for decomposable and non-decomposable sweeps shown on  $\mathcal{F}$ . Here,  $\sigma(p_1) = \sigma(p'_1)$ . The point  $p_0$  is a singular trim point.

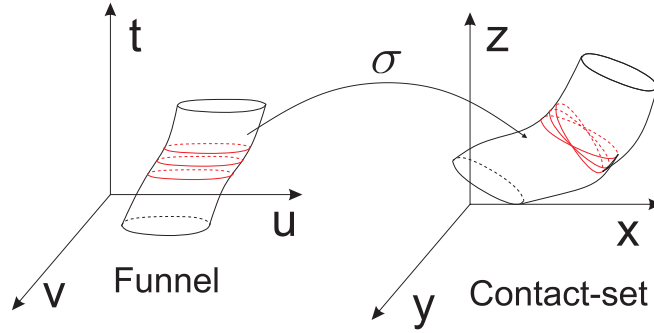


FIGURE 19. A schematic illustrating the interaction between curves of contact in non-decomposable sweeps.

PROPOSITION 43. *If  $p_0 \in \mathcal{F}$  such that  $\theta(p_0) < 0$  then  $p_0 \in pT_I$ .*

*Proof.* Let  $p_0 = (u_0, v_0, t_0) \in \mathcal{F}$ . Recall the definition of the function  $\lambda$  from Equation 6 and relation  $\theta(p_0) = \ddot{\lambda}(t_0)$  from Theorem 40. Clearly, if  $\ddot{\lambda}(t_0) < 0$ , then  $t_0$  is a local maxima of the function  $\lambda$  and the inverse trajectory of  $\sigma(p_0)$  intersects  $M^o(t_0)$  and  $\sigma(p_0) \in T_I$ . Hence, if  $\theta(p_0) < 0$  then  $p_0 \in pT_I$ .  $\square$

Propositions 41 and 43 link the curves of  $\mathcal{F}^0$  to the curves of  $\partial pT_I$ . We see that every curve of  $\mathcal{F}^0$  lies inside a curve of  $\partial pT_I$  and every curve  $C$  of  $\partial pT_I$  has a curve  $\mathcal{F}_C^0$  of  $\mathcal{F}^0$  which makes contact with it. We have already seen that  $\mathcal{F}^0$  is a collection of curves on which  $\nabla\theta$  is non-zero. Thus, the computation of  $\mathcal{F}^0$  in modern kernels is straightforward. The task before us is now to locate the points of  $\mathcal{F}^0 \cap \partial pT_I$  which is enabled by the following function.

DEFINITION 44. Let  $\Omega$  be a parametrization of a curve  $\mathcal{F}_i^0$  of  $\mathcal{F}^0$ . Let  $\Omega(s_0) = p_0 \in \mathcal{F}_i^0$  and  $\bar{z} := (n, m, -1) \in \text{null}(J_\sigma)$  at  $p_0$ , i.e.,  $n\sigma_u + m\sigma_v = \sigma_t$ . Define the function  $\varrho : \mathcal{F}^0 \rightarrow \mathbb{R}$  as follows.

$$(13) \quad \varrho(s_0) = \left\langle \bar{z} \times \frac{d\Omega}{ds} \Big|_{s_0}, \nabla f \Big|_{p_0} \right\rangle$$

where  $\times$  is the cross-product in  $\mathbb{R}^3$ .

Here,  $\varrho$  is a measure of the oriented angle between the tangent at  $p_0$  to  $\mathcal{F}_i^0$  and the kernel (line) of the Jacobian  $J_\sigma$  restricted to the tangent space  $\mathcal{T}_{\mathcal{F}}(p_0)$ .

**PROPOSITION 45.** *Every singular p-trim curve  $C$  makes contact with a curve  $\mathcal{F}_i^0$  of  $\mathcal{F}^0$  so that if  $p_0$  is a singular trim point of  $C$  then  $\varrho(p_0) = 0$ . Furthermore, at such points,  $\varrho'(p_0) \neq 0$  where  $\varrho'$  refers to the derivative of  $\varrho$  along the curve  $\mathcal{F}_i^0$ .*

*Proof.* We know from Proposition 43 that  $\mathcal{F}^- \subset pT_I$ . Since  $\mathcal{F}^0$  and  $\partial pT_I$  form the boundaries of  $\mathcal{F}^-$  and  $pT_I$  respectively,  $\mathcal{F}^0$  and a singular p-trim curve  $C$  of  $\partial pT_I$  meet tangentially at the singular trim point. Further, it was shown in the proof of Proposition 41 that at a singular trim point  $p_0$ ,  $\mathcal{T}_C(p_0)$  is the null-space of the Jacobian  $J_\sigma|_{p_0}$ . Since  $\mathcal{T}_C(p_0) = \mathcal{T}_{\mathcal{F}^0}(p_0)$ ,  $J_\sigma|_{p_0}(\mathcal{T}_{\mathcal{F}^0}(p_0)) = 0$ . Since the function  $\varrho$  measures the oriented angle between  $\text{null}(J_\sigma)$  and  $\mathcal{T}_{\mathcal{F}^0}$ , it follows that  $\varrho(p_0) = 0$ .

The derivative  $\varrho' \neq 0$  at singular trim points for non-decomposable sweeps shown in Figure 16 and Figure 17.  $\square$

The curves of  $\mathcal{F}^0$  can be parametrized via the procedural approach. Further, Proposition 45 confirms that for every singular p-trim curve, we may use the function  $\varrho$  to locate a singular trim point  $p$  in  $\mathcal{F}^0$  in a computationally robust manner. Thus, via  $\theta$  and  $\varrho$  we may access every component of  $\partial pT_I$ .

**PROPOSITION 46.** *In the generic situation, (i) the singular p-trim curve  $C$  has a finite set of singular trim points. Each of these points lie on a curve of  $\mathcal{F}^0$ . (ii) For all but finitely many non-singular points  $p \in C$ , the image  $\sigma(p)$  lies on the transversal intersection of two surface patches  $\sigma(\mathcal{F}_i)$  and the remaining non-singular points lie on intersection of three surface patches  $\sigma(\mathcal{F}_i)$  where  $\mathcal{F}_i \subset \mathcal{F}$  corresponds to the subinterval  $I_i \subset I$ .*

*Proof.* It follows from Proposition 41 that the singular trim points lie on  $\mathcal{F}^0$ . Since at a non-singular trim point  $p \in C$ ,  $\ell(p) > 0$ , the proof for (ii) is identical to the proof for Lemma 30 about elementary trim curves.  $\square$

We now describe the tracing of a singular p-trim curve  $C$  once a point  $p_0$  in  $\mathcal{F}^0$  has been located where  $\varrho$  is zero. Since  $\mathcal{F}^0$  and  $C$  meet tangentially at  $p_0$ , starting at  $p_0$  we take small steps in direction  $\frac{d\Omega}{ds}|_{p_0}$  and  $-\frac{d\Omega}{ds}|_{p_0}$  to obtain points  $\tilde{p}_1$  and  $\tilde{p}'_1$  respectively which are fed to a Newton-Raphson solver which returns points  $p_1$  and  $p'_1$  such that  $p_1, p'_1 \in \mathcal{F}$ ,  $\sigma(p_1) = \sigma(p'_1)$  and  $t(p_1) - t(p'_1) = t(\tilde{p}_1) - t(\tilde{p}'_1)$ . Let  $q_1 := \sigma(p_1) = \sigma(p'_1)$ . Here,  $t(p)$  denotes the  $t$ -coordinate of  $p$ . The point  $q_1$  is on the trim curve and the points  $p_1$  and  $p'_1$  are on the p-trim curve  $C$ . Since points  $p_1$  and  $p'_1$  are non-singular, these can be fed as starting points to any of the known surface-surface intersection algorithms to compute the trim curve.

Note that, for trimming, unlike in the inverse trajectory approach [3, 4], our method does not rely on identifying all the points where  $\theta$  is negative. Further, the funnel being a smooth surface, every point of  $\mathcal{F}$  is accessible via the procedural parametrization (discussed in Appendix C). On this surface, the curve  $\mathcal{F}^0$  is computed. This guarantees that no portion of  $\mathcal{F}^-$  will be left out.

Figure 20 schematically illustrates a scenario in which a singular p-trim curve is nested inside an elementary p-trim curve. Note that the sweep is non-decomposable and this will be detected by the presence of points on  $\mathcal{F}$  where  $\theta \leq 0$ . Further, the region bounded by the singular p-trim curve needs to be excised before a surface-surface intersection algorithm can trace the elementary trim curves since no neighborhood of  $C_I^0$  (where  $\theta$  is zero) can be parametrized. Our analysis will first successfully identify and excise the region bound by the singular p-trim curves.

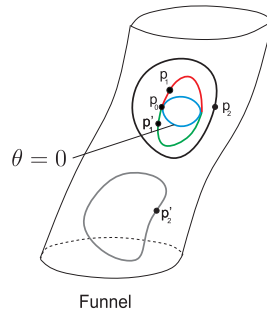


FIGURE 20. A singular p-trim curve nested inside an elementary p-trim curve

After parametrizing the remaining part, the task of excising the regions bound by elementary p-trim curves can be handled by existing kernels.

### 7. Discussion

This paper develops a mathematical framework for the implementation of the “generic” solid sweep in modern solid modelling kernels. This is done via a complete understanding of singularities and of self-intersections within the envelope and the notion of decomposability. This in turn is done through the important invariant  $\theta$  by which all trim-curves are either stable surface-surface intersections or are caught by  $\theta$ .

We now detail certain implementation issues. Firstly, the use of funnel as the parametrization space and the so called “procedural” framework is now standard, see e.g., the ACIS kernel. Secondly, the non-generic case in the sweep, as in blends or surface-surface intersections, will need careful programming and convergence with existing kernel methods for handling degeneracy. Next, while we have not tackled the case when the trim curves intersect the left/right caps, that analysis is not difficult and we skip it for want of space. Finally, the non-smooth sweep is a step away. The local geometry is already available. The trim curves and other combinatorial/topological properties of the smooth and non-smooth case are tackled in a later paper.

Mathematically, our framework may also extend to more complicated cases where the curves of contact are not simple. This calls for a more Morse-theoretic analysis which should yield rich structural insights. The invariant  $\theta$  is surprisingly strong and needs to be studied further.

### Appendix A. Proof for Proposition 8

Recall the statement of Proposition 8 that for  $(y, x, t) \in R$  and  $I = [t_0, t_1]$ , either (i)  $t = t_0$  and  $g(x, t) \leq 0$ , or (ii)  $t = t_1$  and  $g(x, t) \geq 0$  or (iii)  $g(x, t) = 0$ .

*Proof.* Let  $\hat{e}_1, \hat{e}_2, \hat{e}_3$  and  $\hat{e}_4$  be defined as  $(1, 0, 0, 0)$ ,  $(0, 1, 0, 0)$ ,  $(0, 0, 1, 0)$  and  $(0, 0, 0, 1)$  respectively. We define the following objects in  $\mathbb{R}^4$  where the fourth dimension is time. Let  $Z := \{(A(t) \cdot x + b(t), t) \mid x \in M \text{ and } t \in I\}$  and  $X := \{(A(t) \cdot x + b(t), t) \mid x \in \partial M \text{ and } t \in I\}$ . Note that  $Z$  is a four dimensional topological manifold and  $X$  is a three dimensional submanifold of  $Z$ . Further, a point  $(x, t)$  lies in  $Z^\circ$  if  $t \in I^\circ$  and  $x \in M^\circ(t)$ . Further, if  $I = [t_0, t_1]$ ,

$\partial Z = X \cup (M(t_0), t_0) \cup (M(t_1), t_1)$  forms the boundary of  $Z$ . Define the projection  $\mu : \mathbb{R}^3 \times I \rightarrow \mathbb{R}^3$  is defined as  $\mu(x, t) = x$  and the projection  $\tau : \mathbb{R}^3 \times I \rightarrow \mathbb{R}$  is defined as  $\tau(x, t) = t$ . By Lemma 5, for a point  $w \in \mu(Z)$ , if  $\mu^{-1}(w) \cap Z^\circ \neq \emptyset$  then  $w \notin \mathcal{E}$ . Hence a necessary condition for  $w$  to be in  $\mathcal{E}$  is that the line  $\mu^{-1}(w)$  should be tangent to  $\partial Z$  which is a three dimensional manifold which is smooth everywhere except at  $(\partial M(t_0), t_0)$  and at  $(\partial M(t_1), t_1)$ . For  $w \in M^\circ(t_0)$ , the outward normal to  $\partial Z$  at  $(w, t_0)$  is given by  $-\hat{e}_4$  and the outward normal to  $\partial Z$  at  $(w, t_1) \in (M^\circ(t_1), t_1)$  is given by  $\hat{e}_4$ . We now compute the outward normal to  $\partial Z$  at  $(w, t) \in X$ . The manifold  $X$  is diffeomorphic to  $\partial M \times I$ , i.e., the cross product of  $\partial M$  which is a 2-dimensional manifold and  $I$  which is a 1-dimensional manifold, with the diffeomorphism given by  $d : \partial M \times I \rightarrow X$ ,  $d(x, t) = (A(t) \cdot x + b(t), t)$ . Hence, if  $\{y_1, y_2\}$  spans  $\mathcal{T}_{\partial M}(x)$  and  $\{1\}$  spans  $\mathcal{T}_{\mathbb{R}}(t)$  then the tangent space of  $\partial M \times I$  at  $(x, t)$  is spanned by  $\{(y_1, 0), (y_2, 0), \hat{e}_4\}$  and  $\mathcal{T}_X(w, t)$  is spanned by  $\{(A(t) \cdot y_1, 0), (A(t) \cdot y_2, 0), (A'(t) \cdot x + b'(t), 1)\}$ . Hence, the outward normal to  $\partial Z$  at  $(w, t)$  is  $(A(t) \cdot N(x), -\langle A(t) \cdot N(x), v_x(t) \rangle)$ . Consider now three cases as follows.

Case (i):  $t = t_0$ . At any point  $(w, t_0) \in (\partial M(t_0), t_0)$  there is a cone of outward normals given by  $\alpha \begin{bmatrix} A(t) \cdot N(x) \\ -\langle A(t) \cdot N(x), v_x(t) \rangle \end{bmatrix} - \beta \hat{e}_4$  where  $\alpha, \beta \in \mathbb{R}$  and  $\alpha, \beta \geq 0$ . So if the line  $\mu^{-1}(w)$  is tangent to  $\partial Z$  at  $(w, t_0)$  then

$$\left\langle \hat{e}_4, \alpha \begin{bmatrix} A(t) \cdot N(x) \\ -\langle A(t) \cdot N(x), v_x(t) \rangle \end{bmatrix} - \beta \hat{e}_4 \right\rangle = 0$$

for some  $\alpha, \beta$  where  $\alpha > 0$  and  $\beta \geq 0$ . Solving the above for  $\langle A(t) \cdot N(x), v_x(t) \rangle$  we get  $\langle A(t) \cdot N(x), v_x(t) \rangle = -\frac{\beta}{\alpha} \leq 0$ . Hence  $g(x, t) \leq 0$ .

Case (ii):  $t = t_1$ . Proof is similar to case (i).

Case (iii):  $t \in I^\circ$ . If the line  $\mu^{-1}(w)$  is tangent to  $X$  at  $(w, t)$ , we have

$$\left\langle \begin{bmatrix} A(t) \cdot N(x) \\ -\langle A(t) \cdot N(x), v_x(t) \rangle \end{bmatrix}, \hat{e}_4 \right\rangle = 0$$

It follows that  $\langle A(t) \cdot N(x), v_x(t) \rangle = g(x, t) = 0$ .  $\square$

## Appendix B. Some useful facts about the inverse trajectory

Recall the inverse trajectory of a fixed point  $x$  as  $\bar{y}(t) = A^t(t) \cdot (x - b(t))$ . We will denote the trajectory of  $x$  by  $y : [0, 1] \rightarrow \mathbb{R}^3$ ,  $y(t) = A(t) \cdot x + b(t)$ . We now note a few useful facts about  $\bar{y}$ . We assume without loss of generality that  $A(t_0) = I$  and  $b(t_0) = 0$ . Denoting the derivative with respect to  $t$  by  $\dot{\cdot}$ , we have

$$(14) \quad \dot{\bar{y}}(t) = \dot{A}^t(t) \cdot (x - b(t)) - A^t(t) \cdot \dot{b}(t)$$

Since  $A \in SO(3)$  we have,

$$(15) \quad A^t(t) \cdot A(t) = I, \forall t$$

Differentiating Eq. 15 w.r.t.  $t$  we get

$$(16) \quad \dot{A}^t(t_0) + \dot{A}(t_0) = 0$$

$$(17) \quad \ddot{A}^t(t_0) + 2\dot{A}^t(t_0) \cdot \dot{A}(t_0) + \ddot{A}(t_0) = 0$$

Using Eq. 14 and Eq. 16 we get

$$(18) \quad \dot{\bar{y}}(t_0) = -\dot{A}(t_0) \cdot x - \dot{b}(t_0) = -\dot{y}(t_0)$$

Differentiating Eq. 14 w.r.t. time we get

$$(19) \quad \ddot{y}(t) = \ddot{A}^t(t) \cdot (x - b(t)) - 2\dot{A}^t(t) \cdot \dot{b}(t) - A^t(t) \cdot \ddot{b}(t)$$

Using Equations 19, 16 and 17 we get

$$(20) \quad \ddot{y}(t_0) = -\ddot{y}(t_0) + 2\dot{A}(t_0) \cdot \dot{y}(t_0)$$

### Appendix C. Procedural parametrization of the simple sweep

We now describe the parametrization of  $\mathcal{F}$  assuming that the sweep  $(M, h, I)$  is simple. We obtain a procedural parametrization of  $\mathcal{F}$  which is an abstract way of defining curves and surfaces. This approach relies on the fact that from the user's point of view, a parametric surface (curve) in  $\mathbb{R}^3$  is a map from  $\mathbb{R}^2(\mathbb{R})$  to  $\mathbb{R}^3$  and hence is merely a set of programs which allow the user to query the key attributes of the surface (curve), e.g. its domain and to evaluate the surface (curve) and its derivatives at the given parameter value. This approach to defining geometry is especially useful when closed form formulae are not available for the parametrization map and one must resort to iterative numerical methods. We use the Newton-Raphson (NR) method for this purpose. As an example, the parametrization of the intersection  $\bar{y}$  of two surfaces is computed procedurally in [11]. This approach has the advantage of being computationally efficient as well as accurate. For a detailed discussion on the procedural framework, see [12].

The computational framework is as follows. Given  $S$  and  $h$ , an approximate funnel is first computed, which we will refer to as the seed surface. Now, when the user wishes to evaluate  $\mathcal{F}$  or its derivative at some parameter value, a NR method will be started with seed obtained from the seed surface. The NR method will converge, upto the required tolerance, to the required point on  $\mathcal{F}$ , or to its derivative, as required. Here, the precision of the evaluation is only restricted by the finite precision of the computer and hence is accurate. It has the advantage that if a tighter degree of tolerance is required while evaluation of the surface or its derivative, the seed surface does not need to be recomputed. Thus, for the procedural definition of  $\mathcal{F}$  we need the following:

- (1) an NR formulation for computing points on  $\mathcal{F}$  and its derivatives, which we describe in Section C.1
- (2) Seed surface for seeding the NR procedure, which we describe in Section C.2

Recall that  $\mathcal{F} = \bigcup_{t \in I} \mathcal{F}(t)$ . This suggests a natural parametrization of  $\mathcal{F}$  in

which one of the surface parameters is time  $t$ . We will call the other parameter  $p$  and denote the seed surface by  $\bar{\mathcal{F}}$  which is a map from the parameter space of  $\mathcal{F}$  to the parameter space of the sweep map  $\sigma$ , i.e.  $\bar{\mathcal{F}}(p, t) = (\bar{u}(p, t), \bar{v}(p, t), t)$  and while the point  $\bar{\mathcal{F}}(p, t)$  may not belong to  $\mathcal{F}$ , it is close to  $\mathcal{F}$ . We make the following assumption about  $\bar{\mathcal{F}}$ .

**ASSUMPTION 47.** *At every point on the iso-t curve of  $\bar{\mathcal{F}}$ , the normal plane to the iso-t curve intersects the iso-t curve of  $\mathcal{F}$  in exactly one point.*

Note that this is not a very strong assumption and holds true in practice even with rather sparse sampling of points for the seed surface. We now describe the Newton-Raphson formulation for evaluating points on  $\mathcal{F}$  and its derivatives at a given parameter value.

**C.1. NR formulation for  $\mathcal{F}$ .** Recall that the points on  $\mathcal{F}$  were characterized by the tangency condition  $f(u, v, t) = 0$ . Introducing the parameters  $(p, t)$  of  $\mathcal{F}$ , we rewrite this equation  $\forall(p_0, t_0)$ :

$$(21) \quad \begin{aligned} f(u(p_0, t_0), v(p_0, t_0), t_0) &= \langle \hat{N}(u(p_0, t_0), v(p_0, t_0), t_0), \\ &V(u(p_0, t_0), v(p_0, t_0), t_0) \rangle = 0 \end{aligned}$$

So, given  $(p_0, t_0)$ , we have one equation in two unknowns, viz.  $u(p_0, t_0)$  and  $v(p_0, t_0)$ .  $\mathcal{F}(p_0, t_0)$  is defined as the intersection of the plane normal to the iso- $t$  (for  $t = t_0$ ) curve of  $\bar{\mathcal{F}}$  at  $\bar{\mathcal{F}}(p_0, t_0)$  with the iso- $t$  (for  $t = t_0$ ) curve of  $\mathcal{F}$  which is nothing but  $\mathcal{F}(t_0)$ . Recall that  $\mathcal{F}(t_0)$  is given by  $(u(p, t_0), v(p, t_0), t_0)$  where  $u, v, t_0$  obey Eq. 21. Henceforth, we will suppress the notation that  $u, v, \bar{u}$  and  $\bar{v}$  are functions of  $p$  and  $t$ . Also, all the evaluations will be understood to be done at parameter values  $(p_0, t_0)$ . The tangent to iso- $t$  curve of  $\bar{\mathcal{F}}$  at  $(p_0, t_0)$  is given by

$$(22) \quad \frac{\partial \bar{\mathcal{F}}}{\partial p} = \left( \frac{\partial \bar{u}}{\partial p}, \frac{\partial \bar{v}}{\partial p}, 0 \right)$$

Hence,  $\mathcal{F}(p_0, t_0)$  is the solution of simultaneous system of equations 21 and 23

$$(23) \quad \left\langle (u, v, t_0) - (\bar{u}, \bar{v}, t_0), \frac{\partial \bar{\mathcal{F}}}{\partial p} \right\rangle = 0$$

Eq. 21 and Eq. 23 give us a system of two equations in two unknowns,  $u$  and  $v$  and hence can be put into NR framework by computing their first order derivatives w.r.t  $u$  and  $v$ . For any given parameter value  $(p_0, t_0)$ , we seed the NR method with the point  $(\bar{u}(p_0, t_0), \bar{v}(p_0, t_0))$  and solve Eq. 21 and Eq. 23 for  $(u(p_0, t_0), v(p_0, t_0))$  and compute  $\mathcal{F}(p_0, t_0)$ .

Having computed  $\mathcal{F}(p, t)$  we now compute first order derivatives of  $\mathcal{F}$  assuming that they exist. In order to compute  $\frac{\partial \mathcal{F}}{\partial p}$ , we differentiate Eq. 21 and Eq. 23 w.r.t.  $p$  to obtain

$$(24) \quad \left\langle \frac{\partial \hat{N}}{\partial u} \frac{\partial u}{\partial p} + \frac{\partial \hat{N}}{\partial v} \frac{\partial v}{\partial p}, V \right\rangle + \left\langle \hat{N}, \frac{\partial V}{\partial u} \frac{\partial u}{\partial p} + \frac{\partial V}{\partial v} \frac{\partial v}{\partial p} \right\rangle = 0$$

$$(25) \quad \begin{aligned} &\left\langle \left( \frac{\partial u}{\partial p}, \frac{\partial v}{\partial p}, 0 \right) - \left( \frac{\partial \bar{u}}{\partial p}, \frac{\partial \bar{v}}{\partial p}, 0 \right), \frac{\partial \bar{\mathcal{F}}}{\partial p} \right\rangle \\ &+ \left\langle (u, v, t_0) - (\bar{u}, \bar{v}, t_0), \frac{\partial^2 \bar{\mathcal{F}}}{\partial p^2} \right\rangle = 0 \end{aligned}$$

Eq. 24 and Eq. 25 give a system of two equations in two unknowns, viz.,  $\frac{\partial u}{\partial p}$  and  $\frac{\partial v}{\partial p}$  and can be put into NR framework by computing first order derivatives w.r.t.  $\frac{\partial u}{\partial p}$  and  $\frac{\partial v}{\partial p}$ . Note that Eq. 24 and Eq. 25 also involve  $u$  and  $v$  whose computation we have already described. After computing  $\frac{\partial u}{\partial p}$  and  $\frac{\partial v}{\partial p}$ ,  $\frac{\partial \mathcal{F}}{\partial p}$  can be computed as  $(\frac{\partial u}{\partial p}, \frac{\partial v}{\partial p}, 0)$ .  $\frac{\partial \mathcal{F}}{\partial t}$  can similarly be computed by differentiating Eq. 21 and Eq. 23 w.r.t.  $t$ . Higher order derivatives can be computed in a similar manner.

**C.2. Computation of seed surface.** The seed surface is constructed by sampling a few points on the funnel and fitting a tensor product B-spline surface through these points. For this, we first sample a few time instants, say,  $\mathcal{I} = \{t_1, t_2, \dots, t_n\}$  from the time interval of the sweep. For each  $t_i \in \mathcal{I}$ , we sample a few points on the pcurve of contact  $\mathcal{F}(t_i)$ . For this, we begin with one point  $p$  on

$\mathcal{F}(t_i)$  and compute the tangent to  $\mathcal{F}(t_i)$  at  $p$ , call it  $z$ . Then  $p + z$  is used as a seed in Newton-Raphson method to obtain the next point on  $\mathcal{F}(t_i)$  and this process is repeated.

While we do not know of any structured way of choosing the number of sampled points, in practice even a small number of points suffice to ensure that the Assumption 47 is valid.

## References

- [1] Abdel-Malek K, Yeh HJ. Geometric representation of the swept volume using Jacobian rank-deficiency conditions. *Computer-Aided Design* 1997;29(6):457-468.
- [2] ACIS 3D Modeler, SPATIAL, [www.spatial.com/products/3d\\_acis\\_modeling](http://www.spatial.com/products/3d_acis_modeling)
- [3] Blackmore D, Leu MC, Wang L. Sweep-envelope differential equation algorithm and its application to NC machining verification. *Computer-Aided Design* 1997;29(9):629-637.
- [4] Blackmore D, Samulyak R, Leu MC. Trimming swept volumes. *Computer-Aided Design* 1999;31(3):215-223.
- [5] Guillemin V, Pollack A. *Differential Topology*. Prentice-Hall, 1974.
- [6] Heidi E.I.D., Rimvydas Krasauskas. Rational fixed radius rolling ball blends between natural quadrics. *Computer Aided Geometric Design* 2012;29:691-706
- [7] Huseyin Erdim, Horea T. Ilies. Classifying points for sweeping solids. *Computer-Aided Design* 2008;40(9):987-998
- [8] Huseyin Erdim, Horea T. Ilies. Detecting and quantifying envelope singularities in the plane. *Computer-Aided Design* 2007;39(10):829-840
- [9] J. Rossignac, J.J. Kim, S.C. Song, K.C. Suh, C.B. Joungh. Boundary of the volume swept by a free-form solid in screw motion. *Computer-Aided Design* 2007;39; 745-755
- [10] Kinsley Inc. Timing screw for grouping and turning. <https://www.youtube.com/watch?v=LooYoMM5DEo>
- [11] Markot R, Magedson R. Procedural method for evaluating the intersection curves of two parametric surfaces. *Computer-Aided Design* 1990;23(6):395-404
- [12] Milind Sohoni. Computer aided geometric design course notes. [www.cse.iitb.ac.in/~sohoni/336/main.ps](http://www.cse.iitb.ac.in/~sohoni/336/main.ps)
- [13] Peternell M, Pottmann H, Steiner T, Zhao H. Swept volumes. *Computer-Aided Design and Applications* 2005;2;599-608
- [14] Seok Won Lee, Andreas Nestler. Complete swept volume generation, Part I: Swept volume of a piecewise C1-continuous cutter at five-axis milling via Gauss map. *Computer-Aided Design* 2011;43(4):427-441
- [15] Seok Won Lee, Andreas Nestler. Complete swept volume generation, Part II: NC simulation of self-penetration via comprehensive analysis of envelope profiles. *Computer-Aided Design* 2011;43(4):442-456
- [16] Xinyu Zhang, Young J. Kim, Dinesh Manocha. Reliable Sweeps. SPM '09; SIAM/ACM Joint Conference on Geometric and Physical Modeling 2009; 373-378
- [17] Xu Z-Q, Ye X-Z, Chen Z-Y, Zhang Y, Zhang S-Y. Trimming self-intersections in swept volume solid modelling. *Journal of Zhejiang University Science A* 2008;9(4):470-480.